CHALMERS
UNIVERSITY OF TECHNOLOGY

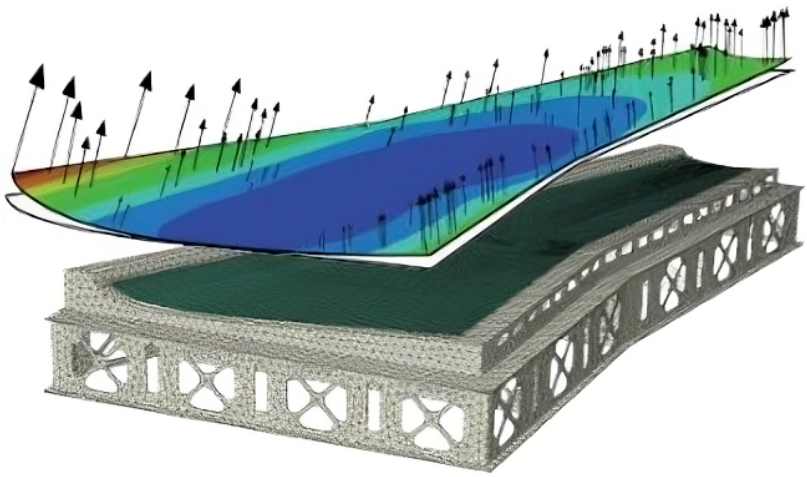

Effect of Tool-Part Interaction in Composite Manufacturing Simulations

Master's thesis in Applied Mechanics

AFRODITI TZANETOU

DEPARTMENT OF INDUSTRIAL AND MATERIALS SCIENCE

CHALMERS UNIVERSITY OF TECHNOLOGY

Gothenburg, Sweden 2024

www.chalmers.se

Master's thesis 2024

Effect of Tool-Part Interaction in Composite Manufacturing Simulations

AFRODITI TZANETOU

CHALMERS
UNIVERSITY OF TECHNOLOGY

Department of Industrial and Materials Science
Chalmers University of Technology
Gothenburg, Sweden 2024

Effect of Tool-Part Interaction in Composite Manufacturing Simulations

AFRODITI TZANETOU

Supervisor: Sibin Saseendran, GKN Aerospace Sweden AB
Examiner: Martin Fagerström, Department of Industrial and Materials Science

Master's Thesis 2024
Department of of Industrial and Materials Science
Chalmers University of Technology
SE-412 96 Gothenburg
Telephone +46 31 772 1000

Cover: Residual stress induced shape distortions in aerospace components

Typeset in LaTeX
Printed by Chalmers Reproservice
Gothenburg, Sweden 2024

Effect of Tool-Part Interaction in Composite Manufacturing Simulations
AFRODITI TZANETOU
Department of Industrial and Materials Science
Chalmers University of Technology

Abstract

Carbon Fiber Reinforced Polymers (CFRP) are widely used across multiple industries, especially in aerospace due to their lightweight and superior specific stiffness and strength. Despite their advantages, their mechanical properties are significantly influenced by the manufacturing process, since factors as the curing process and tool-part interactions are critical in the development of defects like shape distortions.

Examining the critical parameters of CFRP manufacturing process with a focus on of tool-part interaction, the main goal of this master thesis is the development of validated methods for Finite Element (FE) models to investigate the process-induced distortions and predict the tool effect on the processing. In the frame of this project, L-shaped CFRP components are manufactured and FE models are built-up in LS-DYNA simulating the curing and demolding process of the composites so as to predict the resulting shape distortions in terms of spring-in and warpage. The FE simulations are validated using measurements from the manufactured components, and the numerical results are analysed aiming to assess the impact of tool-part interaction on process-induced distortions. The goal is to determine whether this interaction significantly influences the distortions, justifying its consideration in future studies.

The results of this master thesis indicate the importance of selecting a high-fidelity material model in numerical simulations, since linear material models poorly predict spring-in and warpage when compared to experimental results. Using a simplified composite constituent model, the FE simulation is inadequate for capturing the tool effect and the tool-part contact simulation becomes ineffective. Implementation of more efficient methods to numerically measure spring-in and warpage are recommended to enhance the FE validation process. Additionally, experimental results suggest that titanium tools induce more significant deviations from the flat composite surface than steel tools, while asymmetric laminates exhibit considerably higher warpage than quasi-isotropic and unidirectional ones. Based on these findings, a re-evaluation of the assumptions made in this study is also suggested, so as the FE simulations developed in this work can be recognised as a precise tool for accurate spring-in and warpage prediction.

Keywords: CFRP, L-shaped composites, Finite element model validation, tool-part interaction, curing process, spring-in, warpage

Acknowledgements

First and foremost, I would like to express my sincere gratitude to my master thesis supervisor, Sibin Saseendran, for his continuous support and guidance throughout this period. His expertise in composites analysis and simulation, along with his encouragement, greatly fueled my enthusiasm and deepened my knowledge in the field. I am also thankful for the opportunity to join the Composites Team at GKN Aerospace Sweden. Additionally, I extend my thanks to all my colleagues at GKN Aerospace Sweden for their valuable insights into composite simulations and their expertise and guidance in composites manufacturing during the experimental phase of my thesis.

I am also grateful to Martin Fagerström, my thesis examiner, for his advanced guidance and support. His deep knowledge in finite elements was instrumental in developing advanced simulation methods. My thanks also go to the PhD students at the Department of Industrial and Materials Science at Chalmers University of Technology for their insightful comments, which significantly improved my master thesis work.

A special thanks to Anders Bernhardsson at Ansys for his support in troubleshooting and improving the FE models throughout this process. His expertise and willingness to share detailed explanations of his suggested LS-DYNA simulation methods have been immensely appreciated.

Lastly, I would like to thank Kenneth Strand at RISE Research Institutes of Sweden for performing the 3D scanning of the manufactured composites and providing insightful explanations on the measurement methods used, which greatly assisted in improving the FE model validation process.

Afroditi Tzanetou
Gothenburg, August 2024

List of Acronyms

Below is the list of acronyms that have been used throughout this thesis listed in alphabetical order:

CLT	Classical Lamination Theory
CSC	Chemical Shrinkage Coefficient
CTE	Coefficient of Thermal Expansion
DoC	Degree of Cure
DoF	Degree of Freedom
FE	Finite Element
PID	Process-Induced Distortion
UD	Unidirectional
CFRP	Carbon Fiber Reinforced Polymer

Contents

List of Figures

List of Tables

1
Introduction

1.1 Background

Carbon Fiber Reinforced Polymers (CFRP) are extensively utilized in various industrial applications, particularly in the aerospace industry that increasingly relies on CFRP for its lightweight characteristics compared to its high stiffness and strength. However, apart from the anisotropic nature of composite materials that poses challenges in manufacturing large and complex shapes, the mechanical properties of carbon fiber composites are highly affected by the manufacturing process. Parameters as the cure process and tool-part interaction play a significant role in the development of process-induced defects (PIDs), such as residual stresses and shape distortions.

In the aerospace sector, constructing composite structures raise the need of precise alignment of their smaller constituent parts during assembly. Inaccurate dimensions of these parts can prolong assembly duration as well as increase costs. A primary cause of such inaccuracies in composite components is the accumulation of residual stress during the curing process, leading to distortions upon the removal of the part from the manufacturing tool. In particular, these inaccuracies in dimensions lead to increased expenses due to increased assembly efforts as, for complex structures assembled from multiple parts, manual adjustments are often necessary to eliminate gaps between neighboring components. Moreover, the option of redesigning tools is usually not efficient since this extends lead times of the production process. Therefore, there is a need in the industry for fast and cost-efficient PID prediction methodologies that can be used early in the design process to assess dimensional fidelity.

As a result of several studies, tool-part interaction has been identified as the main reason for flat and curved laminates to present PIDs after curing [1, 2, 3]. Research on the PIDs of composite parts has been extended over the last 25 years, with various predictive techniques explored in literature [3, 4, 5, 6, 7, 8, 9]. Analytical solutions offer insights into residual stress and distortion mechanisms using the CLT or energy methods to predict the shape of laminates after curing. Additionally, the Finite Element (FE) method has become a well-established approach for modeling residual stress, thermal effects and shape distortions in composite components. However, in order for this numerical method to predict accurate results, demands on extensive experimental methods as well as material characterization often exist, in addition to high computational resources.

1.2 Main purpose

As in aerospace it is significant to predict and mitigate process-induced defects in order to avoid costly trial-and-error methods, the main purpose of this master thesis is the investigation of the critical parameters of CFRP manufacturing process affecting distortions with a focus on of tool-part interaction. Aim of the study is the assessment of the influence of tool-part interaction in distortions, determining whether it should be considered in future researches.

1.3 Goals

The main goal of this study is to develop and validate FE models to predict shape distortions, focusing on the effects form tool-part interactions. In the frame of this master thesis, L-shaped CFRP components are manufactured and their material properties are characterized. Finite element models are developed in LS-DYNA software to perform process simulations predicting the outcome of the manufacturing methods in terms of shape distortions of the composite part. The FE simulations are validated using measurements from the manufactured components and the numerical results are analysed.

1.4 Limitations

The limitations of this master's thesis study are mainly related to assumptions made in the developed FE model for coupled thermal-structural analysis, as numerical simulations and material models inherently involve simplifications that limit the accuracy of predictions. In particular:

- For the heat transfer analysis, it was presumed that the tool and the part were in perfect contact and that any deformations of the tool and the part were assumed to have no influence in the temperature field.
- External environmental factors, such as temperature and humidity variations during the manufacturing process of L-shaped CFRP components, are not considered in the simulations. The simulations utilize a uniform and homogeneous temperature on the surfaces of the tool-composite assembly exposed in the air of the oven. This temperature field is considered to be identical to the one recorded by the thermocouple positioned on the tool during the curing process. However, the temperature is not considered uniform through the thickness of the composite and tool parts.
- The current study does not consider inter-ply slippage resulting from tool-part interaction as a contributing factor to the PIDs. In reality, the layer nearest to the tool experiences the greatest deflection, as a result from both the transfer of shear stress between the plies and inter-ply slippage, leading to curvature in each layer. However, the latter phenomenon is not taken into account in the scope of this study.
- For the two metal tools used for the manufacturing, the materials are considered to follow linear elastic isotropic behavior. Therefore, the tool's Coefficient

of Thermal Expansion (CTE) is assumed to remain constant throughout the curing process, and no potential directional CTE resulting from the tool manufacturing process is explored.
- The precision of the L-shaped tools used for the manufacturing was not verified, and the angles were assumed to be at 90 degrees with high precision.
- For this investigation, the interaction between the tool and the part was simulated by employing static and dynamic friction coefficients that are independent of the curing process and temperature change.
- Human factors like operator skills during the ply stack-up process are not accounted for in this study. Although effects such as small misalignment of plies can influence the occurrence of defects in CFRP components such as deviations in laminate thickness, they cannot be replicated in the virtual model.
- Regarding the validation of the FE model, errors associated with the accuracy of the 3D scanner are not taken into account.

2
Theory

2.1 State of the art

2.1.1 Fiber-Reinforced Composites

Composite materials, including polymer-matrix composites, are widely employed across various industries as aircraft, marine vessels, and electric powered automobiles due to their exceptional mechanical benefits. In particular, in aerospace applications polymer-matrix composites are increasingly favored due to their numerous advantages over conventional metals such as aluminum. These include their lightweight nature, high strength-to-weight ratio, directional strength, resistance to corrosion, low thermal conductivity and CTE, as well as their minimal maintenance requirements.

FRP, or Fiber Reinforced Polymer, is described as a polymer matrix, which can be either thermoset or thermoplastic, reinforced with fibers or other reinforcing materials characterized by a significant aspect ratio (length to thickness ratio) to offer notable reinforcement in one or more directions. Its properties are primarily evident in the direction of the applied load [10].

At the compositional level, resin polymer serves as the 'glue' that holds the composites together playing a crucial role in determining the physical characteristics of the final product. Its primary function involves transferring stresses between the reinforcing fibers, acting as an adhesive to hold the fibers together, providing protection against mechanical and environmental damage.

Two major categories of resins exists; thermoset and thermoplastic. Thermoplastic resins are typically in liquid or low-melting point solid form initially. Upon application, these resins are "cured" using a catalyst, heat, or a combination of both to produce finished products. Once cured, thermoset resins do not melt and flow but rather soften when heated. They subsequently become rigid after cooling and, once formed, they cannot be reshaped or revert to their original liquid state [10]. Common thermoset resins utilized in the composites industry include unsaturated polyesters, epoxies, vinyl esters, and phenolics.

The reinforcement component is the one providing the mechanical strength to the composite material. Fibers or reinforcements primarily function to bear load along their length, thereby providing strength and stiffness in a specific direction. These

fibers can be oriented at various angles within the polymer matrix. They are offered in diverse forms such as roving, milled fiber, chopped strands, etc., produced by a wide spectrum of processes so as to be employed for different end-product applications. Typically, fiberglass or carbon materials are utilized for FRPs.

Prepreg is a ready-made composite material consisting of reinforcement forms of "pre-impregnated" fibers and a partially cured polymer matrix, such as epoxy or resin. Prepregs are produced by passing reinforcing fibers or forms, like fabrics, through a resin bath to saturate or impregnate the fiber, followed by heating to advance the curing reaction to different stages. They are available in thermoset or thermoplastic forms and can be stored either in a refrigerator or at room temperature, depending on the constituent materials. Prepregs offer versatility in application, allowing for manual or mechanical application at various directions as per design requirements [10].

Laminates are assemblies of layers of composite materials such as prepreg plies, which are joined together. These individual layers typically demonstrate anisotropic, orthotropic, or quasi-isotropic behavior.

Anisotropy in composites arises from different factors, including the fiber orientation (aligned or continuous) in the subsequent plies of the laminate and the distribution of fibers across the geometry of the product. This anisotropy can be categorized into "in-plane" and "out-of-plane" to analyze the variations in properties along different directions within the material. The material's anisotropic behavior is affected by the properties of its constituent elements, such as stiffness and CTE.

Orthotropic laminates are characterized by their ability to deform similarly to an orthotropic UD ply when subjected to loading along material axes. These laminates can consist of UD plies all oriented in the same direction, cross-ply plies oriented at 0 or 90 degrees to the reference axis, or angle-ply laminates with an equal number of plies oriented at $\pm\ \theta$ angles. Notably, orthotropic laminates exhibit no coupling between normal stresses and shear strain.

Quasi-isotropic laminates demonstrate isotropic responses within the plane, but their out-of-plane responses are not necessarily isotropic. The laminate's lay-up of individual plies determines whether coupling between in-plane and out-of-plane responses occurs. Achieving in-plane quasi-isotropic behavior involves stacking plies at various orientations, although a distinction persists in out-of-plane behavior.

In structural applications, laminates are typically designed to be symmetric and balanced. In symmetric laminates, the bending and extension of the laminate are decoupled. Balanced laminates feature an equal amount of off-axis angle plies, which helps to reduce shear coupling.

Overall, FRP composites are highly versatile offering multiple benefits for their application. The final properties of a product are highly influenced by the type of

materials chosen and the manufacturing process employed. The selection of materials depends on the desired performance and intended usage of the product, since critical factors such as the choice of fiber reinforcement, fiber volume, orientation of fibers, and the type of resin used significantly impact the properties of the laminate. By considering the significance of interplay between material selection and manufacturing techniques in defining the attributes of the end product, composite designers can optimize the performance of it to meet the specific requirements. Hence, it's essential for end-users to have solid understanding on the application environment, load performance, and durability requirements, so as to effectively convey this information to professionals within the composites industry.

2.1.2 Physical and Mechanical properties of Thermosetting Composites

Thermosetting composites are widely utilized for manufacturing of aircraft components as they have excellent resistance at temperatures between 50 and 100° C, can withstand high stress and present lightweight properties compared to many metals. Epoxy and phenolic resins are the ones that are most commonly used in aerospace industry, and their micro-structure is responsible for their properties and, hence, the thermosetting composite part properties.

Thermosetting composites begin as a mixture of fiber reinforcement and unreacted resin, which is placed between molds or on a single mold surface. The resin is initially at a monomer state. Under elevated temperature with the aid of accelerator, the resin then undergoes polymerization and cross-linking reactions leading to strong bonds between the molecules.

As the resin reacts, it undergoes phase transitions. In particular, the material transitions from a liquid-like viscous state to a rubber-like state, and finally to visco-elastic solid that is called as glassy state. Heat is released during that process. Once the resin has cured, both the composite and the molds are cooled to room temperature, and the composite part is then removed from the molds.

The extent of this phase transformation is measured by the Degree of Cure (DoC). The value of DoC is ranging from 0 to 1, where 0 indicates no curing and 1 represents a fully cured state with no remaining free monomer units to react [10]. Since the chemical reactions are exothermal, the DoC in the material can be estimated by measuring the released heat using a Differential Scanning Calorimeter equipment.

The amorphous structure of thermosetting polymers is defined by a glass transition temperature (T_g), also called gelation temperature, which determines the approximate temperature at which the cured resin will significantly soften and yield under load [10]. In practice, T_g is affected from parameters such as the polymer type, and it is used to define the temperature limit at which the composite can safely operate. As shown in Figure 2.1, T_g depends on DoC starting from T_{g0} for the thermoset being at a liquid-like viscous state reaching its maximum value $T_{g\infty}$ when it is fully

cured.

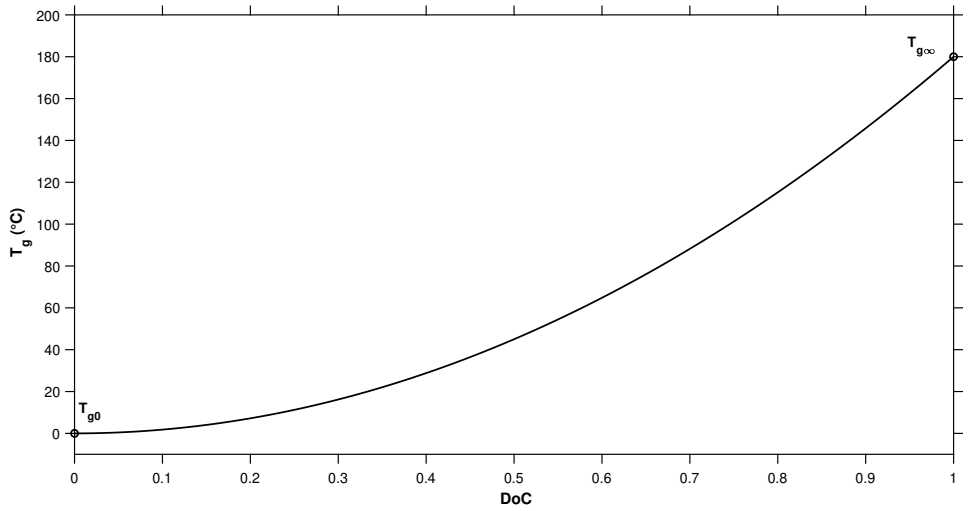

Figure 2.1: Glass transition temperature with degree of cure development for thermosetting composites, qualitative graph.

Although the mechanical properties of thermosets are less influenced by temperature changes compared to thermoplastics, there is still a variation in properties such as the Young's modulus or CTE. For instance, as illustrated in Figure 2.2, below T_g the Young's modulus of the thermoset is in a glassy state and a constant glassy stiffness E_g can be assumed. When T_g is exceeded the resin transforms into a rubbery state and the composite stiffness modulus reduces to an assumed rubbery stiffness E_r.

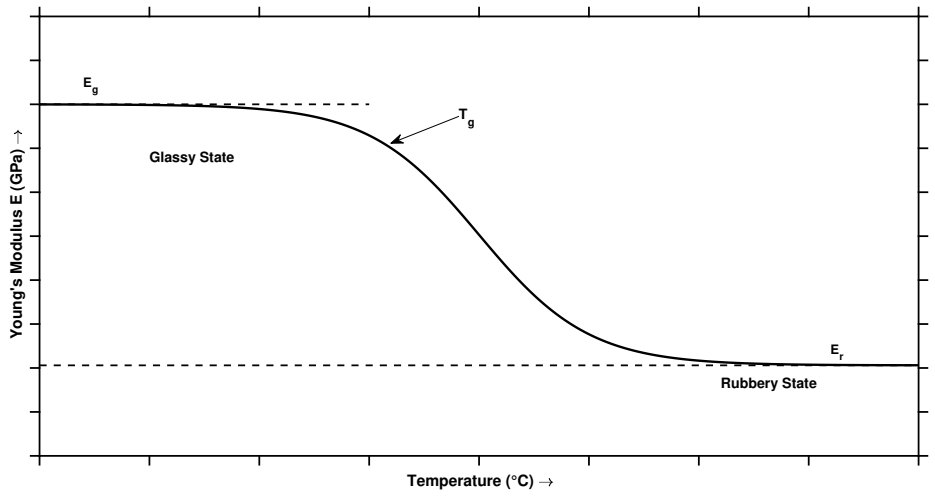

Figure 2.2: Young's Modulus with temperature development for thermosetting composites, qualitative graph.

Since composites exhibit visco-elastic behavior, they are characterized by both immediate elastic deformation as well as time-dependent responses on applied stress

and strains. That means that the mechanical properties of the material are time-dependent. Higher temperatures also tend to increase the viscous behavior of the material. Especially at elevated temperatures and low DoC, stress relaxation or creep phenomena may occur. In particular, stress relaxation is denoted as time-dependent stress change after rapid loading under constant strain conditions. Complementary to this behavior, under rapid constant stress loading at an elevated temperature conditions is denoted as creep.

Therefore, in order to accurately predict the mechanical behavior of the composite materials it is important to utilize methods that describe efficiently their curing process as well as capture the visco-elastic phenomena they exhibit. The development of a constitutive law for different composite materials is a complex process and consists a field of study of many researchers as it is discussed in a following section.

2.2 Manufacturing and Process Induced Distortions

2.2.1 Curing Process of Composites

Composite parts are produced using a variety of methods, with the most common for high-quality applications being resin transfer molding, injection molding and the prepreg process. In the latter method, prepregs, which are sheets already impregnated with resin, are subjected to curing process during which a chemical reaction or heat treatment takes place to solidify the composite material and form the desired properties and shape.

During the curing of prepreg composites, prepreg sheets are initially hand-laid onto a mold or laid onto a tool surface using numerically controlled prepreg-placement machine. Then, the composite laminate is covered with various bagging materials such as bleeder layers, breather cloths, or vacuum bags. Afterwards, the curing process begins, with the assembly being placed in an autoclave or a curing oven machine and subjected to a controlled cycle of temperature and pressure until the composite is completely cured. As a last step, finishing of the part's surfaces follows.

The advantage of prepreg process technique is that, in case of automated ply placement methods are used, the ply layups can be arranged on the mold precisely according to requirements ensuring a high-quality product. However, a disadvantage is that prepreg sheets are partially cured and must be stored in a climate-controlled environment to prevent them from fully curing over time, which would render them hard and unusable [10]. In addition, residual stresses are often developed in the formed part upon demolding, which lead in deviations in the shape of manufactured part from the shape of the tool from which it was laid up upon removal [5]. To address this latter issue, understanding the main mechanisms that take place during the curing process is essential.

Curing is a complex, coupled thermo-mechanical and chemical process marked by significant heat generation and changes in the material's mechanical properties [10]. During curing, thermally and chemically induced volumetric strains generate residual stresses. Initially, tool-part interaction mechanisms create stresses due to differential strains between the part and the tooling on which it is fabricated. For instance, aluminum or steel tools, with higher CTE values compared to composite parts, stretch the composite as they heat up, causing small shear stresses at the tool interface that induce tension in the part.

As the curing process progresses, the prepreg material is subjected to controlled cycles of heat and pressure. Once the resin vitrifies and achieves significant stiffness, it begins to behave like an elastic solid and no additional effects resulting from tool interaction occur. During this phase, the magnitude of chemical shrinkage strain is comparable to that of thermal strain and can, therefore, be addressed in a similar way [11]. Thermal stresses and associated distortions emerge from this stage onward.

These stresses, depending on the process and the tool characteristics used, can result in PIDs in the produced parts or initiate microscopic cracks [10].

There are also other mechanisms acting during curing, for instance, associated with moisture as well as to variations in fiber volume fraction throughout the thickness. The movement of fibers during the curing process can induce changes in geometry and properties too, resulting in stresses and distortion [11].However, the focus of this study will remain on the thermal and chemical shrinkage strains, as well as tool-part interaction mechanisms, which contribute most significantly to residual stresses and PIDs.

2.2.2 Residual Stresses and Process Induced Distortions

Process-induced distortions are associated with two distinct deformation mechanisms, spring-in and warpage. The two phenomena, which are studied in more detail to a following section in this thesis, coexist in composite structures, and PIDs are considered to be the combined effect of those [12].

A thorough understanding of the sources inducing residual stresses and PIDs is essential for manufacturing parts with improved dimensional accuracy and for minimizing the residual stresses that arise in the parts during the manufacturing process [13]. For this purpose, in the following paragraphs the mechanisms are classified and studied based on their source and scale occurring.

The origins of residual stresses that lead to shape distortions in composite parts can be traced to various factors which, for a source-based classification, can be broadly categorized into intrinsic and extrinsic. Both intrinsic and extrinsic sources can have a contribution to process-induced distortions.

Intrinsic factors are related to the resin's properties, such as chemical shrinkage and thermal expansion, the thermal expansion properties of fibers, part geometry, and lay-up, all of which are defined by the design engineer [14]. The material selection process during the part design is often dominant in determining material-related parameters, including the Chemical Shrinkage Coefficient (CSC) of the resin and the mismatch between the CTE of resin and fiber, as well as in inducing anisotropic mechanical properties in the composite [15]. Furthermore, the intrinsic behavior of selected polymer matrix determines in a significant extent the anisotropic intrinsic behavior of the composite material [10]. In particular, phenomena occurring in polymer behavior and processing, typically creep and stress relaxation phenomena, are also present to varying degrees at the composite level depending on volume fraction of matrix in the part.

Extrinsic factors are directly related to the tooling and manufacturing process, and are generally managed by the process engineer and can be modified without involving design engineers or stress analysts [14]. These parameters include the design, material and surface of the tool, the bagging arrangement, the process equipment

such as ovens, autoclaves, and presses used, as well as the cure cycle that the composite is subjected to [15]. Extrinsic sources are significantly affected by the thermal and mechanical tool-part interaction. In particular, the thermal interaction with the tool translates into thermal gradients through the laminate thickness, that result in through-thickness stress gradients (residual stresses). Mechanical interaction involves stresses induced in a composite part due to the deformability of tools and mismatches in the thermal expansion of tool and part materials.

For a scale-based classification, during composite processing various micro- to component-level mechanisms lead to the formation of residual stresses and, therefore, PIDs. Residual stresses in composite structures generally fall into three categories as mismatches occur at various scales. Firstly, examining the micro-level between the fiber and matrix constituents, microscopic stresses exist between the fiber and resin within each ply. Secondly, at the meso-level between plies with different orientations, macroscopic stresses arise at the ply-to-ply scale due to anisotropic differences in CTEs or chemical shrinkage. Finally, at the macro-level between the part and the tool, where structural scale residual stresses occur from variations in shrinkage through the thickness of structures due to friction and other geometric constraints [1, 2]. However, in most of the literature studies residual stresses in composites are studied and classified as into two categories; micromechanical residual stresses and macromechanical residual stresses, with the latter ones to be responsible for large-scale dimensional changes [5, 10].

Micromechanical stresses in thermoset composites arise within a single fiber-matrix composite, mainly due to the anisotropy and heterogeneity of the composite. The residual stresses develop between the fiber and matrix, primarily due to the mismatch in CTEs and Young's modulus between the fiber and matrix, result in differences in thermal expansion strains. The expansion coefficient of polymer-matrix materials is generally much higher than that of the fibers, and many fibers have orthotropic expansion coefficients. For example, carbon fibers have very low or slightly negative expansion coefficients in the fiber direction but higher values in the transverse direction. This discrepancy creates residual stresses at the microscale during cool-down, even in unidirectional materials.

In addition, the micro-level strains resulting from resin shrinkage during curing also contribute in the development of micromechanical stresses and distortions. These distortions come as a result of thermosets presenting changes in their mechanical properties during curing due to temperature variations throughout the curing process. Notably, although the evaluation of micro residual stresses as well as the assessment of their local effects is a quite challenging process, they do not significantly affect large-scale deformations [10].

On the macromechanical level, individual plies can be regarded as anisotropic but homogeneous layers. It is known from literature [10] that, in a ply level, stresses are typically assumed to vary continuously within each ply. However, anisotropic material contraction is taking place during curing due to the chemical shrinkage

of the resin. Specifically, this ansiotropic contraction is caused as the fibers do not shrink and resist the laminate's contraction along their principal directions. Consequently, the in-plane chemical shrinkage of the entire laminate is lower than the through-thickness shrinkage, functioning similarly to CTE-related contraction and causing comparable stress and distortion conditions.

In a laminate level, the development of residual stresses starts during the early stages of the curing cycle. At this stage, the resin is in a rubbery state, with its mechanical stiffness defined by the rubbery modulus. That means that the composite material's shear modulus is very low because the resin's polymeric chains are not yet linked. As the tool and composite part are pressed together under autoclave pressure and subjected to a temperature increase, the applied pressure pushes the laminate against the rigid mold. While the tool and part are compressed together, they attempt to expand or contract relative to each other. However, the mold, having typically higher CTE, expands more than the composite part. This mismatch in CTEs results to tool-material interaction forces arising along with cure shrinkage and thermal strain, as well as generation of shear stresses at the mold-laminate interface. Due to the low shear modulus of the composite and poor stress transfer through its thickness, the plies in contact with the mold experience the most strain, resulting to the generation of stress gradient through the laminate thickness. In a macro-scale level, the tool-part interaction places the laminate in tension, as it is stretched due to the expansion of the tool [5, 15].

As the resin vitrifies and transitions to a glassy solid, the shear modulus significantly increases locking the non-uniform stress distribution and deformations in the laminate that induced in the earlier curing stage. Upon demolding, the autoclave pressure and mold restraints are removed, by releasing the boundary conditions from the composite part [16]. At this stage, when the cured part is removed from the mold, these frozen stresses are released allowing the part to deform freely as it cools down to room temperature [17]. This results to increased bending moments which cause the part to warp away from the tool [15].

It is noteworthy that the laminate geometry and lay-up can have significant effect in the generation of PIDs. For flat geometry plates, if the lay-ups are not balanced and symmetric with respect to the mid-plane, residual stresses will build up, but they will not lead to significant distortions. In this case, discontinuities may occur between plies as the macromechanical residual stresses will be generated during cooling from the high curing temperature [5]. For instance, it is well-known that asymmetric cross-ply laminates exhibit curvature, and angle plies can lead to twisting. In contrast, curved plates are prone to distortion even when the lay-up is balanced and symmetric, due to the effective shift of the neutral axis caused by the curvature [11, 18].

Vacuum bag technology amplifies the effects of the interaction between the laminate and the mold. By this curing method, only one surface of the laminate is subjected to the rigid mold while the other is in contact with the flexible vacuum bag, which

has less effect in the generated shear stress field within the laminate. This differential interaction further contributes to the development of residual stresses and distortions [17].

Besides the aforementioned parameters primarily due to mismatches in CTE in either microscale or macroscale level, it has been observed that the magnitude and distribution of residual stress is also influenced by a variety of other factors. Contributing factors are related to the cure cycle, the curing kinetics of the matrix, as well as to variations in fiber volume ratio, uneven resin flow or initial defects in the material such as fiber wrinkling [10, 19, 20]. Other sources of through-thickness stress gradient involve the magnitude of autoclave pressure cycle applied during the curing process, and the non-uniform cooling of the laminate due to severe temperature gradients as there is temperature difference between the upper and lower laminate surface, particularly applicable in single-sided mould concepts [3, 5]. Last but not least, the condition of the tool surface related to friction conditions that are necessary to transfer stress between the two contacting surfaces, as well as the tool-part interaction in terms of heat transfer within the part and the tool and at their boundaries are among the other factors contributing to residual stress [1].

Consequently, in addition to material costs due to rejections of parts, manufacturing distortions pose a significant challenge to the widespread industrial usage of thermoset composite structures as they necessitate intensive assembly efforts. To mitigate these issues and achieve cost-effective manufacturing of large and reliably stiff composite structures, accurate prediction of the final shape and cure-induced distortions, such as spring-in for curved composite parts is crucial [3, 6].

2.2.3 Spring-in and Warpage phenomena in L-shaped Composites

Typically, in practical applications, curved composite parts such as L, T, C and U shapes are more commonly utilized compared to flat components. Therefore, the focus of this section is on studying and quantitatively describe the spring-in and warpage effect in L-shaped parts.

In particular, although composite plies exhibit a transversely isotropic CTE, the related stresses do not cause deformations if they can self-equilibrate. This occurs in case of a flat symmetrical and balanced laminate. However, compared to a flat composite panel, a non-planar composite part is more prone to distortion even when the layups are balanced and symmetric as its curvature shifts the neutral axis of the section, preventing residual stresses from self-equilibrating [6, 17]. It is known that in typical laminate layups, such as cross-ply or quasi-isotropic configurations, in-plane free-strains are minimal compared to through-thickness free-strains. Consequently, around curved corners, residual stresses form, causing dimensional changes. Upon demolding, these process-induced residual stresses are partially released, leading to bending deformations such as spring-in angles and warpage [1].

Spring-in is defined as the reduction of a part's flange-to-flange angle from its nominal (design) value [12, 17]. Typically, the term is used to to describe the closing of angles and the increase in curvature of any curved section, such as L-profiles. Since it is primarily driven by intrinsic factors, spring-in is considered to be the most critical phenomenon, as it affects nearly every CFRP structure [14].

According to the definition, the angle of the composite part after release from the tool $\theta^{'}$ is smaller than the angle in the tool θ, as shown in Figure 2.3. Therefore, in this study, the spring-in angle for the part is expressed as $\Delta\theta = \theta^{'} - \theta$ [2].

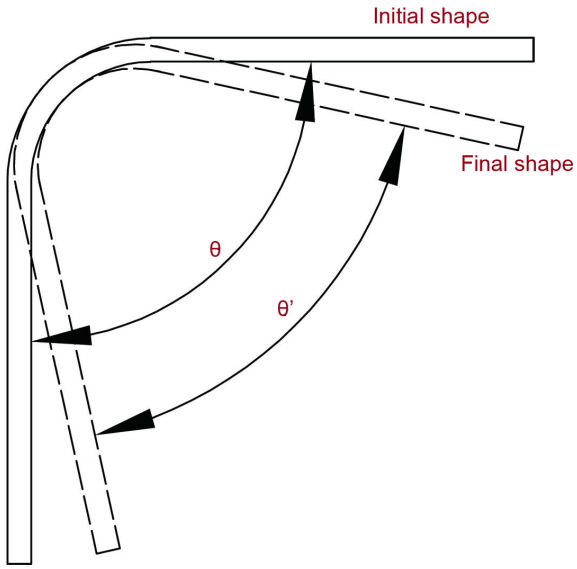

Figure 2.3: Spring-in phenomenon in the L-shaped composite part [2].

Upon separation of the L-shaped part from the tool, the constrained bending moment generated in the rubbery state is released, converting the frozen rotation angle into an equal and opposite spring-in angle. A more pronounced frozen bending moment results in a more significant spring-in after demolding [6].

The mechanisms of spring-in can be classified into two components: thermoelastic and non-thermoelastic. Thermoelastic spring-in refers to the shape change in a macrosale level caused by the higher CTE through-the-thickness direction (dominated by the matrix) compared the in-plane ones (dominated by the fibers). It is reversible, meaning that the part expands when heated up to the process temperature and contracts back to its initial shape when it is cooled back to room temperature. In contrast, the non-thermoelastic component can be attributed to phenomena that occur during the curing process [18]. As the deformations due to chemical shrinkage are irreversible, this spring-in component is also called chemo-thermoelastic. Overall, spring-in is primarily influenced by chemo-thermoelastic mechanisms, referring to the anisotropy of laminate shrinkage in-plane versus through thickness. This anisotropy is mainly determined by the significant chemical shrinkage of the resin and its high CTE compared to the fibers [14].

Extensive experimental studies on the spring-in phenomenon have revealed that the occurrence of spring-in in laboratory-scale L-profile specimens depends on various other factors including the curing process, layup, tooling properties, as well as the composite material itself [14]. Other studies [6] experimentally demonstrate that the length of the flange (the straight component of an L-shaped part) as well as the laminate thickness [12] is a crucial parameter influencing the spring-in of L-shaped parts. The fiber volume fraction can also impact spring-in, as it has been observed [19] that the effect of fiber volume gradient on spring-in is minimal for thicker parts compared to thinner ones.

Warpage is defined as the deviation from flatness (curving) of initially flat sections or the change in the curvature of the part after manufacturing [3, 12]. The definition refers to process-induced stress gradients which cause an in-plane to out-of-plane coupling that can lead to out-of-plane deformation even in orthotropic and symmetric laminates [3, 10]. As a result, the manufactured laminate presents a deviation from their intended plane shape, with an example illustrated in Figure 2.4. As indicated in previous studies, warpage is mainly caused by extrinsic sources [14].

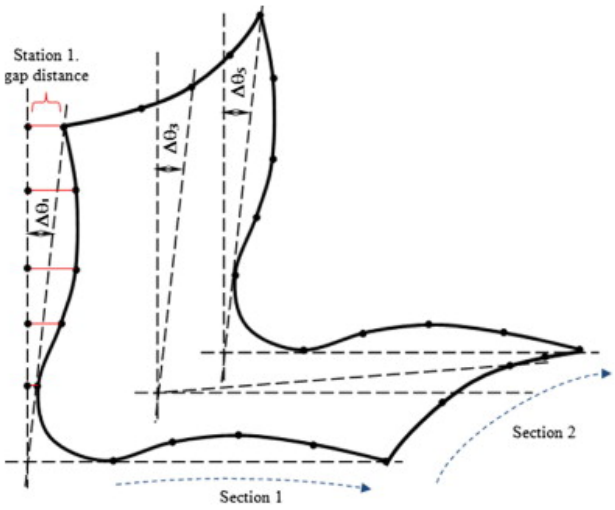

Figure 2.4: Schematic representation of warpage deformation pattern in L-shaped composite part [19].

Several parameters were found to influence the process-induced warpage, with tool–part interaction to be the main mechanism [3]. Typically warpage distortion arises from a mismatch in CTE between the tool and the composite material. This CTE difference causes a stress distribution through the thickness of the composite that becomes locked-in as the composite cures and transitions to a more or less elastic state, stretching of the part at the interface between the tool and the part [14]. Subsequently, this stress distribution is partially released in the form of warpage.

Forming a composite into or onto a corner mold introduces a bending strain profile, where fiber bundles are compressed in the smaller radius and extended and flattened in the larger radius. This can cause resin migration, leading to a through-thickness

redistribution of the fiber volume fraction and resulting in a distribution of the anisotropic properties. This redistribution creates a non-symmetry in the lay-up, which can lead to warpage [10].

Other studies focus in examining different extrinsic process-related parameters affecting warpage, like the rate of application and the magnitude of applied pressure and temperature [7], friction between the part and the tool [14], as well as the effect of release agent or film used [13]. There are also researches on the influence of intrinsic factors influencing warpage as through-thickness fiber volume fraction gradients, lay-up orientation, part thickness and shape, prepreg age or resin viscosity.

Attention is also given to the effect of uneven curing and resin flow in warpage distortion of curved part, particularly in thick composite parts and around corners. Specifically, thermal gradients are typically minimal during the heating and curing processes for thin composite laminates, that consequently lead to small gradients in thermal expansion and chemical shrinkage. However, in the case of thick parts the exothermic heat generated can lead to a through-thickness temperature gradient. This variation in temperature can cause differences in the extent of cure across the thickness. Additionally, if non-symmetric thermal conditions exist on the top and bottom laminate surfaces, the resulting stress profile can induce warpage [10].

Overall, residual stresses can lead to a reduction in apparent strength or even failure before demolding, while spring-in and warpage that are frequently induced during composite manufacturing can render a component useless. These shape distortions can potentially decrease mechanical performance and result to significant geometry mismatches in assembly of large and complex parts, necessitating manufacturers to employ labor-intensive or expensive compensation techniques like shimming to meet tolerance requirements [1]. Hence, achieving precise dimensional control is important in the manufacturing of large composite parts [21].

For this purpose, significant efforts have been directed towards developing simulation tools capable of predicting residual stresses and shape distortions prior to manufacturing the first component. For the prediction of shape distortions, an efficient approach involves utilizing process simulation using FE analysis to mitigate these dimensional changes by compensating tool geometry or optimizing process parameters. For this strategy to be effective, robust methods are needed to accurately characterize the primary mechanisms contributing to these dimensional changes [22]. Following this approach, the focus of this study is on examining the effects of parameters related to tool-part interaction on the spring-in and warpage dimensional distortions.

2.3 Constituent Models for Composite Applications

Cure simulation is a valuable tool for predicting PIDs, process-induced stresses and strains in composite components, since its usage aids in the limitation of the often costly experimental methods [23]. Compared to traditional analytical methods, numerical simulations using FE can more efficiently and accurately predict the development of residual stresses, enabling improved structural designs with lower residual stresses.

The selection of constitutive laws is critical for achieving accurate FE results. Various mathematical methods, including the conventional elastic model, modified elastic models such as the Cure Hardening Instantaneous Linear Elastic (CHILE) model [24] and visco-elastic models, have been developed to calculate residual stresses and predict PIDs in composite structures [2]. The presentation of the most common ones used in studies follows, along with a discretion of the fundamental theory behind the LS-DYNA built-in material model that is utilized in the developed FE simulations of this thesis.

2.3.1 Material Models in Literature

Elastic material models utilize Hooke's law. They focus on predicting PIDs during the cooling phase of the curing cycle, when the material has reached its final DoC with the assumption that it follows elastic behavior at this stage [9]. The simplest model, assuming Hookean material behaviour, is described by the constitutive equations [2.1] and [2.2].

$$\sigma_i = E_{ij}\,\epsilon_j \tag{2.1}$$

In this equation, σ_i and ϵ_i represent the stress and strain vectors in Voigt notation, respectively, while E_{ij} denotes the stiffness matrix. Specifically, the strain vector is decomposed into thermal and shrinkage components:

$$\begin{aligned} \epsilon_i &= \epsilon_i^{thermal} + \epsilon_i^{shrinkage} \\ \epsilon_i^{thermal} &= \beta_i\,\Delta T \\ \epsilon_i^{shrinkage} &= \gamma_i\,\Delta\alpha \end{aligned} \tag{2.2}$$

Here, β_i and γ_i are the vectors for the thermal expansion coefficient and shrinkage coefficient in Voigt notation, respectively. ΔT and $\Delta\alpha$ represent the changes in temperature and DoC.

In studies where an elastic material model is utilized, the numerical prediction of residual stresses depend solely on the final cool-down stage using an elastic constitutive law, assuming that residual stresses arise from thermal strain during this stage. The elastic model, combined with Classical Lamination Theory (CLT) or modified CLT, can effectively predict residual stresses in thin laminates. However, since this model is limited to the cool-down stage, it cannot accurately predict residual stresses

in thick laminates where the complexities of the DoC and temperature variations are more difficult to be captured. Moreover, the elastic model does not account for the variation in the components of the stiffness tensor with temperature or DoC. This variation is crucial for describing the transition of the polymer component from a rubbery to a glassy state [2].

To address these issues, a modified elastic model known as CHILE [24] was proposed to consider temperature and degree of cure gradients throughout the curing process. The CHILE model accounts for Young's modulus development during curing as a function of temperature and DoC. Described by the constitutive equation [2.3] for the relaxation time τ, this model is instantaneously elastic meaning that the material behavior is considered elastic at each time step.

$$\sigma_i(T,\alpha) = \int_0^t E_{ij}(T,\alpha)\frac{d\epsilon_j}{d\tau}\,d\tau \tag{2.3}$$

In particular, in this material model the curing history is divided into three stages, as shown in Figure 2.5. In the first one, the resin is in a viscous flow (liquid) state. In the second stage identified by the gel point, the curing of resin is intense and its elastic modulus rapidly increases and the resin volume shrinks. In the last stage, a fully cured state is considered for the resin with no further chemical reactions taking place.

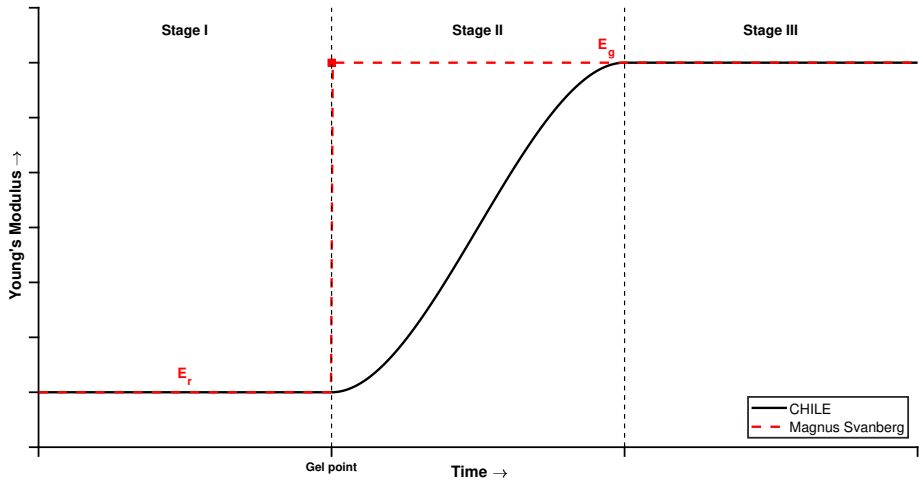

Figure 2.5: Young's modulus development during composite's curing, qualitative graph.

The CHILE model has been widely used by researchers and serves as a benchmark for developing other modified elastic material models such as the one presented by Svanberg [25]. In Svanberg's research, instead of considering the Young's modulus development during curing as a function of temperature and DoC, a simplified elastic material model is developed based on the concept that the curing process

can be split into two segments, assigning a constant elastic modulus to each segment for calculating residual stresses. As is qualitatively described in Figure 2.5, a rubbery modulus is taken into account below the gel point while a glassy modulus is considered at the gel point and after that. Since for this moduli transition the material loading history is taken into account, the material model of Svanberg can be described as pseudo-visco-elastic.

Due to its simplicity in FE implementation, the CHILE model has become popular for theoretical and experimental analyses of residual stress evolution during curing [9, 20]. However the CHILE model, as well as the modified elastic models inspired from that, remains an instantaneously elastic model unable to account for stress relaxation phenomena at high temperatures and low degrees of cure during due to its lack of time dependency [9]. It is also noteworthy that, according to the experimental and numerical results of research [9], the modified CHILE material model overestimates the spring-in angle for the majority of the cases examined in the particular study.

To account for time-dependent factors like heating and cooling rates, stress relaxation, and cure time, visco-elastic material models are suitable to provide more accurate FE predictions. In such an approach, under the assumption of small strains, the visco-elastic phenomena, such as stress relaxation in composite can be modeled as a time-dependent function. Based on the Time-Temprature-Cure Superposition Theorem, the constitute relation is described from equation [2.4] as:

$$\sigma_i(t) = \int_0^t E_{ij}(\xi - \xi^{'}) \frac{d\epsilon_j}{d\tau} \cdot d\tau \tag{2.4}$$

where ξ and $\xi^{'}$ are the reduced times.

Early visco-elastic analyses of residual stresses and PIDs in composite structures, utilize visco-elastic constitutive models assuming thermo-rheologically simple materials, meaning that the glassy and rubbery Young's modulus are independent of temperature and degree of cure. In order to more accurately predict the residual stresses and PIDs by considering temperature-dependent properties of polymer matrices, including CTEs, cure behaviors, and stress relaxation, the so called thermo-visco-elastic models have been developed. In [2], a thermo-visco-elastic law that considers the thermal dependence on residual stresses during curing is proposed. The study focuses on deriving a more general formulation of a three-dimensional integral thermo-visco-elastic constitutive law and corresponding incremental finite element code associated with the macroscopic residual stresses generated during curing. Considering temperature factors, thermal expansions, chemical shrinkage, and stress relaxation, the incremental form of the constitutive law is implemented as user-material (UMAT) in ABAQUS CAE software, describing the visco-elastic behavior of isotropic or orthotropic materials subjected to varying temperatures during curing. In [26] a visco-elastic 'VisCoR' material model describing complex thermo-rheological behavior is developed as, apart from the dependency on temperature and DoC, the derived novel model contains three cure and temperature

dependent functions.

Overall, it is important to highlight the differences in accuracy of predictions, numerical complexity and cost between the various constitutive models. Generally, the cooling process is elastic since the composite is in the glassy state, making it relatively straightforward to capture the material behavior in this stage. As the chemical curing process affects the material parameters development, the accuracy of the simulation primarily depends on this stage. This is the reason that the primary focus of material modeling efforts lies in tracking the evolution of resin properties during the curing process, as the properties of the fibers undergo minimal change throughout manufacturing [9, 23].

Therefore, since the composites are visco-elastic materials and not elastic, the elastic models considering a constant moduli are the ones with the lower accuracy, although they are often used in studies due to their least computational effort compared to the more complicated ones. The modified elastic models, characterized by a moduli that varies with temperature and DoC, offer relatively higher accuracy and, hence, computational cost. To achieve a more accurate prediction of the residual stresses and PIDs as well as effectively capture the material's response throughout the curing cycle, visco-elastic, or thermo-visco-elastic are necessary, in which the moduli vary with temprature, DoC but with time as well. However, as it is reasonable, the complex representation of the material behavior during curing is accompanied with high computational cost.

Despite the significant research efforts in this field, accurately estimating process-induced deformation in complex geometries remains an ongoing challenge. This difficulty arises from the numerous factors that contribute to PID, such as the variability of process conditions and material properties [9]. The input of appropriate material parameters, such as composite shrinkage strain and stiffness changes during curing, is crucial for an accurate simulation of the curing composite. In addition, the validation of the simulation is a key factor for improving the accuracy of the simulation [23].

2.3.2 LS-DYNA Material Model for Composite Cure Kinetics

The material model that is used in the FE simulations of this master thesis is provided as a built-in material model for the LS-DYNA software. In particular, the material type 21, as given in the LS-DYNA Materials Manual [27], describes a linearly elastic orthotropic material with orthotropic CTE parameters. The material model is also able to take into account the curing parameters such as CSC for orthotropic properties.

As an elastic material, the Hooke's law is followed with the constitutive equation described by the second Piola-Kirchhoff stress $\mathbf{S}$ and the Green St. Venant strain $\mathbf{E}$ tensors, as:

$$\mathbf{S} = \mathbf{C} : \mathbf{E} = \mathbf{T}^T \mathbf{C_l}\, \mathbf{T} : \mathbf{E}, \tag{2.5}$$

where $\mathbf{T}$ is the transformation matrix, and $\mathbf{C_l}$ is the constitutive matrix defined in terms of the orthotropic material properties of Young's modulus, Poisson's ratio and shear modulus which are considered to be constant in this material model.

The incremented form of the local thermal strain component for the current time step n, is computed in the longitudinal a, transverse b and through-thickness c direction as:

$$\begin{aligned} \epsilon_{aa}^{n+1} &= \epsilon_{aa}^{n} + \beta_a(T^{n+1} - T^n) \\ \epsilon_{bb}^{n+1} &= \epsilon_{bb}^{n} + \beta_b(T^{n+1} - T^n) \\ \epsilon_{cc}^{n+1} &= \epsilon_{cc}^{n} + \beta_c(T^{n+1} - T^n) \end{aligned} \tag{2.6}$$

The corresponding formulas for the chemical strain components are:

$$\begin{aligned} \epsilon_{aa}^{n+1} &= \epsilon_{aa}^{n} + \gamma_a(\alpha^{n+1} - \alpha^n) \\ \epsilon_{bb}^{n+1} &= \epsilon_{bb}^{n} + \gamma_b(\alpha^{n+1} - \alpha^n) \\ \epsilon_{cc}^{n+1} &= \epsilon_{cc}^{n} + \gamma_c(\alpha^{n+1} - \alpha^n) \end{aligned} \tag{2.7}$$

where α is computed as an internal material variable using the Kamal model. Notably, the β and γ values can be inserted in the material model either as constant either as functions of DoC. Since the material model is provided by the commercial software, more information for it are available in the LS-DYNA Material Manual.

2.4 Tool-Part Interaction in Composite Analysis

2.4.1 Literature Review for Tool-Composite Interaction

Several studies which have explored tool-part interaction during composites curing reveal that significantly affects the residual stresses and distortions in the components [2, 10]. Although some mechanisms related to tool-composite interaction are well-studied and understood, others remain highly uncertain as attempts related to their understanding and mitigation are still performed through experience-based methods.

According to many studies, such as [1], tool-part interaction is the primary cause of warpage. The findings of Zappino et al. [1] reveal that the maximum warpage is highly sensitive to interfacial shear stress, with an increase in shear stress leading to a linear increase in warpage. Stefaniak et al. [3] conclude that tool–part interaction related to mismatch of CTE between the tool and part is a crucial factor in process-induced deformations of flat and symmetric laminates. This mismatch, combined with the curing oven pressure which forces the part and tooling together, causes a non-uniform stress distribution that is locked in as the resin cures. The study findings in [22] highlight that the number of release coats as well as the cure pressure and temperature, significantly affect tool-part interaction by changing the surface conditions and visco-elastic response at the tool-part interface. Additionally, the findings of the study suggest that incorporating 45° plies near the tool-part interface can help reduce residual stresses during curing. Kappel et al. [4] examine tool-part interaction in terms of surface roughness between the parts in contact, revealing that it highly affects warpage distortion.

2.4.2 Boundary Conditions and Contact at Tool-Part Interface

A crucial aspect to the successful modelling of PIDs is the accurate representation of the mechanical boundary conditions to which the curing composite is subjected. The methods by which the shear interaction along the tool–composite interface is simulated can significantly influence the accuracy of model predictions [8]. Hence, the focus of this master thesis is on the accurate numerical representation of the tool-composite interaction, in terms of proper definition of the boundary and contact conditions between the surfaces interacting in a FE model.

In literature, different approaches have been followed for simulating the tool-part interaction with the aim of studying PIDs. In many studies, such as in [9, 17, 25], the tool-part interaction was completely neglected assuming a freely sliding interface (frictionless contact) between the tool and composite. This assumption was followed since several non-stick coatings are applied on the tool, making its surface very smooth and leading to free tangential displacements at the interface allowing the composite to expand and contract freely. However, according to researches [9, 25], this approach tends to overestimate the shape distortion values.

In the contrary, there are several studies were the tool-composite interaction was considered and modeled using assumptions such as the perfectly-bonded interfacial condition [9, 25], the frictional interface model (frictional contact) [9, 21, 28, 29] or by utilizing a fictitious shear-layer [8, 30].

Examining the perfectly-bonded interaction approach, fixed mechanical boundary condition were applied at the nodes of the interface assuming that the composite is stuck to the tool surface without any relative motion. This method, followed in [9], implies that all the translational DoFs of either the composite surface nodes that would be in contact with the tool either all composite nodes, are set to zero until the cool down step is complete. A demolding step is then added to the simulation when the fixed mechanical boundary condition is deactivated and the composite is free to deform, with boundary conditions acting to suppress the parts' rigid body motion. According to studies [9, 25], this approach tends to underestimate the shape distortions.

It is noteworthy that, according to similar studies, the frictionless contact or perfectly-bonded modeling approaches are not considered very accurate approaches. In [29] it is concluded that the level of interaction at the tool–part interface cannot be simulated with the frictionless or perfectly-bonded interface, since the tool and composite prepreg surfaces are not smooth due to surface roughness, fiber diameter and architecture. As a result, it is suggested to use a frictional contact interface instead. In agreement to this study, researchers in [21] support that despite the application of non-stick coating on the tool surface, the composite part seldom expands or contracts freely on the tool. It is also claimed that the fixed mechanical boundary condition approach does not allow the proper simulation of the slip between the tool and the composite, as it overly restricts movement and can result in violations of realistic contact conditions. For a more realistic calculation of the tool-composite which can relative slip due to press against each other but cannot pass through or penetrate one another, the use of a frictional interface model is suggested with the definition of thermal contact condition in the interface. Lastly, findings of study [9] reveal that for most of the tests conducted the values for the tool-part-interaction prediction for the spring-in lie between the fixed boundary condition and frictionless contact cases, offering a more accurate result compared to the experiments.

Considering the above, a frictional model approach could be a more accurate representation of the tool-part interface, highlighting the importance of simulating the tool part in the FE model rather than replacing it with boundary conditions.

Examining the frictional contact approach, a contact condition is defined in the tool-part interface. In most models this is often described by a "hard" contact relationship in the normal interface direction to prevent the transfer of tensile stresses across the interface and to minimize surface interpenetration [28], and a stick–slip behaviour in the tangential direction following the classical Coulomb friction model. According to this model, the interfacial shear stress is proportional to the contact pressure with the CoF as the constant of proportionality. The proportionality is

maintained until a critical shear stress is reached, and the surfaces in contact start to slide under a constant critical shear stress value. In many studies, as in [9], a constant CoF is employed in the tangential direction, while more advanced approaches exist such measuring the CoF experimentally [28] or defining it as cure-dependent [21].

A different frictional FE modeling approach is, instead of employing a sliding friction condition at the tool–part interface, to simulate the tool–part shear interaction by incorporating an elastic shear layer between the tool and part. By adjusting the modulus of the elements in this layer, the amount of stress transferred between tool and composite could be tailored since, depending on the value assigned to the elastic modulus of the shear layer, a range of tool-part interface conditions can be simulated [8]. It is noteworthy that Twigg et al. [8] concluded that simulation results were significantly affected on the shear layer properties with the PIDs of the composite laminate to vary several orders of magnitude. Other researchers [30] base the shear layer properties to calibrated values from experimental PID measurements as well as to semi-empirical models.

Concluding, researches reveal that a frictional contact model tends to be more accurate representation of the tool-composite interaction. Several studies focused on developing FE models using commercial software for solving the numerical problem and validating the results with experimental measurements. However, the number of the studies developing an FE model for LS-DYNA is significantly limited. Considering the above, in this thesis project the simplified assumption of perfectly-bonded boundary condition is compared with the frictional contact condition, in FE models developed for LS-DYNA.

3
Methods

Since trial and error is a time consuming and costly process to be performed in order to appropriately understand and measure the PIDs, this thesis instead performed a comparison between numerical and experimental results. This is an approach that has been extensively used in literature for studying similar problems, with its robustness and accuracy to be significantly affected by factors in the FE model such as the constitutive laws utilized, the FE mesh, as well as the contact and boundary conditions definition.

With the aim of studying the spring-in and warpage phenomena, manufacturing of L-shaped CFRP components were performed in GKN Aerospace facilities. Two tools were used for the manufacturing, one of titanium material made of additive manufacturing process, and one of conventional steel sheet. Four different L-profiles were manufactured consisting of sixteen plies each, in particular of unidirectional laminates $[0]_{16}$ and $[90]_{16}$, quasi-isotropic laminates of $[0/\pm 45/90/0/\pm 45/90]_S$ and asymmetric laminates of $[0/\pm 45/90/0/\mp 45/90]_2$. Overall, the manufacturing of 8 L-profile components took place, and prepreg AS4 material was used for all of the laminates. The purpose of this step is to experimentally examine the influence of the manufacturing tool and laminate lay-up in the resulting warpage and spring-in of the laminate.

The next step was to scan the eight L-shaped components in order to measure the spring-in angle and warpage in each of them, that occurred as defects in the geometry of the components during the curing process. The scanning was performed by the Research Institute of Sweden (RISE AB), and the measured PIDs served as a benchmark for the FE model validation.

Finite element models were developed for simulating the curing process of the L-shaped composite laminates, with the primary goal of examining PIDs as a result of tool-part interaction. The study aimed to determine whether the simulation of tool part is necessary for a more accurate PID prediction or it could be replaced by a mechanical boundary conditions on the composite. Additionally, in case the FE models including the tool-composite simulation, the question to be answered is whether a 'tied' contact algorithm is more representative compared a sliding one.

To address these questions, three different FE models were built-up for each of the eight components, investigating the effect of fixed and contact boundary conditions on PIDs. The first model involved only the composite component, where fixed

boundary conditions were applied to the surface that would typically contact the tool. The remaining two FE models, include the simulation of both the tool (steel or titanium) and composite parts, describing the composite-tool interface using a 'tied' or sliding contact algorithm.

The CAD models for the laminates and tool were initially designed using Siemens NX software. The geometry was then imported into Ansys ACP and Ansys Mechanical, which served as the pre-processing tools for setting up the numerical simulations to be solved in LS-DYNA.

3.1 Manufacturing and Analysis of L-shaped Composites

In the following subsection the manufacturing and curing process of the eight composite parts is described, for the four lay-ups that were hand-laid onto the two tools, shown in Figures 3.1 and 3.2.

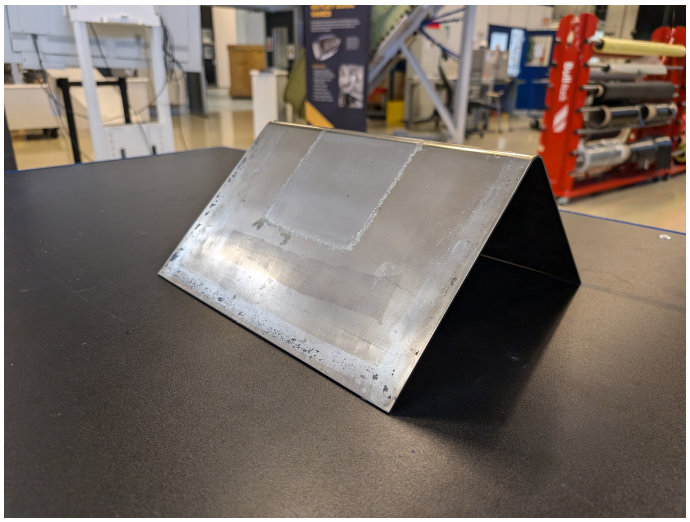

Figure 3.1: Tool made of steel material used for the manufacturing of four laminates.

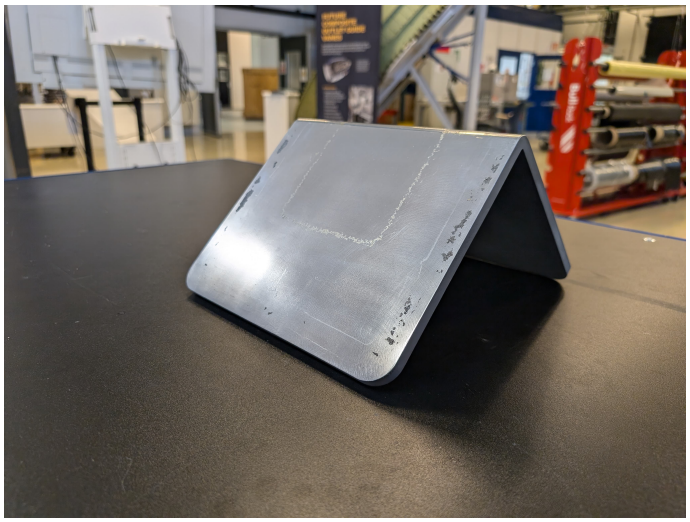

Figure 3.2: Tool made of titanium material used for the manufacturing of four laminates.

The process started with the preparation of the tool. As a first step, sealing of the tool surface was performed by applying four coats of Marbocote Mould Sealer. Then, the application of three coats of Marbocote 227CEE followed to achieve free sliding between of prepreg in contact with the tool and easy removal of produced

part from the tooling at the end of cure cycle. Next the hand-laid process began, for stacking-up the first eight out of the sixteen CFRP prepreg on the tool surface to form an L-shaped stack, as shown in Figure 3.3 (a). Each ply was carefully laid-up, with special attention given to aligning the fibers correctly and preventing wrinkle formation. Specifically, the long side of the tool was designated as the zero-degree fiber direction. When the lay-up process of eight plies was completed, Teflon high temperature (210 ° C) release film of 13 μm thickness was applied over the surface of the prepreg stack, shown in Figure 3.3 (b). This film acted as separator between the prepreg and the fabric breather, which was placed next in order to absorb the excess resin during curing, illustrated in Figure 3.3 (c). As a following step, the tool-part assembly was covered with a vacuum bag with the aid of a sealant tape. By this manner, vacuum was created as the entrapped air bubbles were removed, resulting to an early compaction of the prepreg stack.

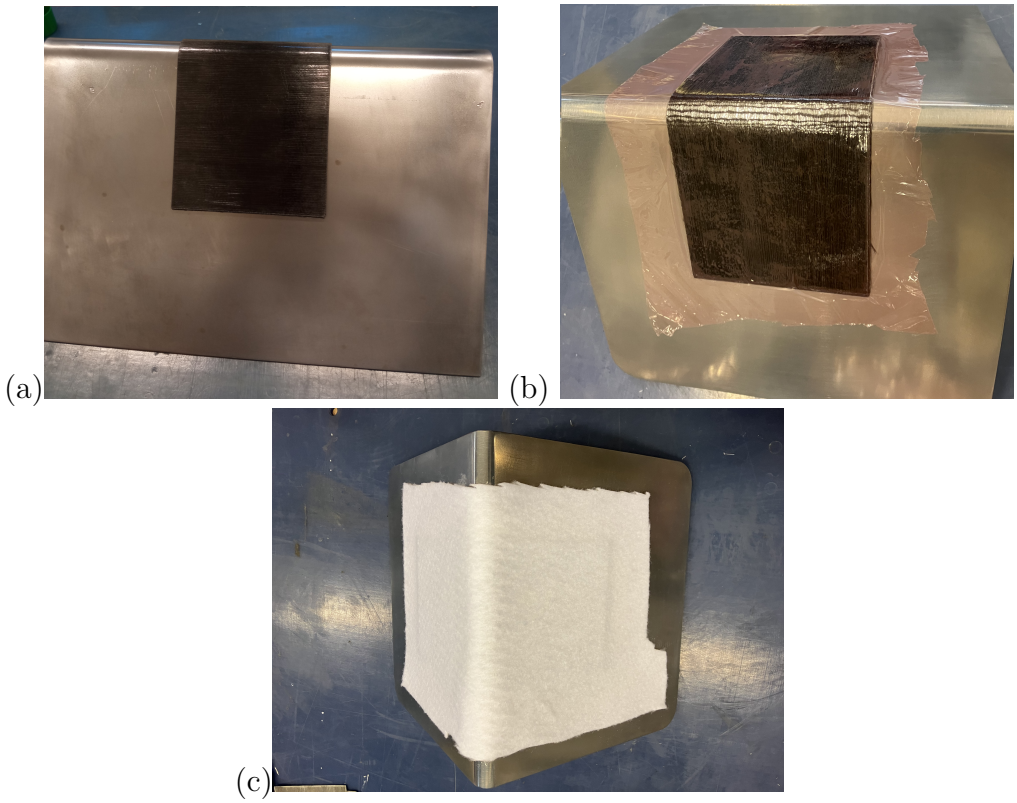

Figure 3.3: (a) Hand lay-up of prepregs on L-shaped tool, (b) covering the prepgregs with release film, and (c) covering with fabric breather.

The vacuum bag, the release film and the breather were then removed and the remaining eight plies were hand-laid onto the tool. Covering again the stack-up with a new release film, fabric breather and vacuum bag material, the entrapped air was again removed and the entire assembly was placed in the curing oven, as shown in Figure 3.4. The curing process then started, as the assembly was subjected to a controlled cycle of temperature till the composite became fully cured. At the beginning the temperature was 20 ° C, then increased to 180 ° C within 1 hour and,

after holding it constant for 2 hours, the process temperature decreased back to 20 ° C within 1 hour.

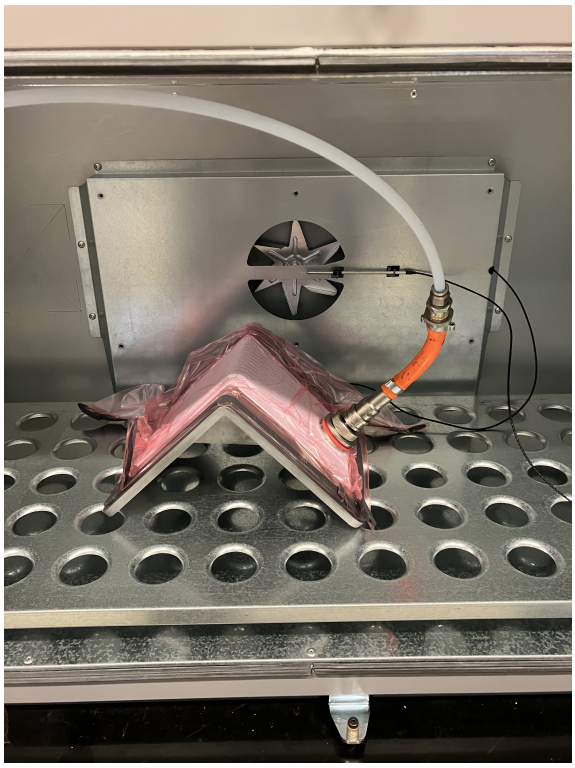

Figure 3.4: Tool-composite assembly covered with vacuum bag and placed in curing oven.

A thermocouple was used for data collection for the temperature rate during the curing process of of L-profile components. The thermocouple, held in place with high-temperature tape, was placed on the underside surface of the tool near the tool corner to measure the air temperature at this location. After the cure cycle was completed and the tool had been cooled down to room temperature, the part was extracted from the tool and its edges were trimmed. One of the produced L-shaped laminates is shown in Figure 3.5.

This process was repeated eight times, as unidirectional laminates $[0]_{16}$ and $[90]_{16}$, quasi-isotropic laminates of $[0/\pm 45/90/0/\pm 45/90]_S$ and asymmetric laminates of $[0/\pm 45/90/0/\mp 45/90]_2$ were manufactured on a titanium and a steel material tool respectively.

It must be noted here that the plies were cut using an automated machine to ensure their the accurate dimensions. However, the prepregs were stacked manually on the tools without any laser projection method. This process may lead to fibre reorientation during the handing and, thus, affecting the induced distortions. In addition, defects in the corner region were detected in some of the specimens. These defects were neglected in the developed simulation.

Figure 3.5: Manufactured L-shaped composite, $[0]_{16}$ using titanium tool.

After the manufacturing of the 8 L-shaped components was complete, the components were scanned using equipment ATOS Q 8M in order to measure the spring-in angle and the distortion of each component that occurred as defects in the geometry of the components during the curing process. The measurements are presented in Results section, in comparison with the numerical results.

3.2 Simulation of Curing Process of L-profile Components

3.2.1 FE Models Goal and Description

The complex physical nature of process-induced distortions necessitates the use of FE analyses to investigate their values, since analytical models often poorly correlate with the experimental results. It is noteworthy that observations from previous studies [28] of manufactured composite parts demonstrate that the deformation of L- and U-shaped parts is not constant along the length direction, meaning that a 2D section assuming a plain strain model does not represent the true nature of the deformation of the part. Therefore, in this study a 3D FE model was developed to predict the shape distortions for L-profile composites.

Hence, for the purposes of this study, different FE models were built-up performing coupled thermo-mechanical analysis. First, only the composite part was considered and the tool-part interaction was simulated using boundary conditions on the surface of the composite that would come in contact with the tool. Next, FE models including the composite part laid on the titanium and steel material tool were developed, respectively. In the latter cases the tool-part interaction was approached in a more realistic manner compared to the first model, with the contact between them to be simulated. All the FE models were then analysed for the four different composite lay-ups.

The FE models simulate the curing and demolding process of the composite. Initially, the uncured L-shaped composite part was laid onto a tool part. This interaction was either represented with boundary conditions and absence of the tool from the simulation, either with a contact between them. Starting from room temperature, the tool-part assembly was subjected to the temperature cycle till the composite is fully solidified. During this time the L-shaped part is also under a vacuum pressure. When the curing process ends, demolding of the composite follows. As it is has no more interaction with the tool and subjected to no pressure, the composite is free to distort. The spring-in and warpage distortions can be obtained numerically by calculating the change in angle and deviation from the initially flat composite flange respectively.

It must be noted here that generally linear FE models were developed in order to reduce the complexity of the problem, while the source of non-linearity was the contact definition in whichever of the FE models this was applicable. However, in terms of this master thesis, the option of using a non-linear material model was explored as well. At an initial state of this thesis work, a non-linear user-defined material model was utilized [26], which was able to describe the phase change of the composite and capture the visco-elasticity phenomena. However, convergence issues of the FE models and time constraints lead to its replacement with a linear built-in material model for LS-DYNA solver.

3.2.2 FE Models Build-up

3.2.2.1 Geometry and Materials

Describing the geometry of the FE models that were built-up, the composite part of total thickness 3.04 mm, 215 mm length and 100 mm width was simulated with an angle of 90°, as shown in Figure 3.6.

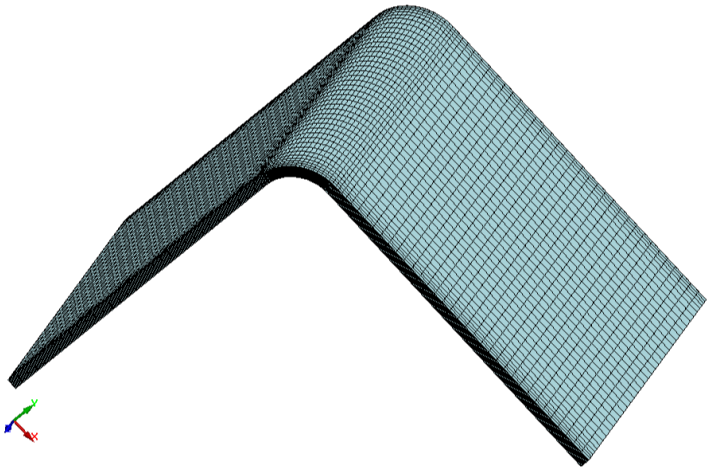

Figure 3.6: FE model where only the composite part is simulated, corresponding to laminates made using titanium tool.

Since the radius of the two corner tools used for the manufacturing is slightly different, the inner radius of the composite is designed to 12 mm for laminates made using the the titanium tool and 14 mm for the ones using the steel tool. The tool-composite FE models are depicted in Figures 3.7 and 3.8.

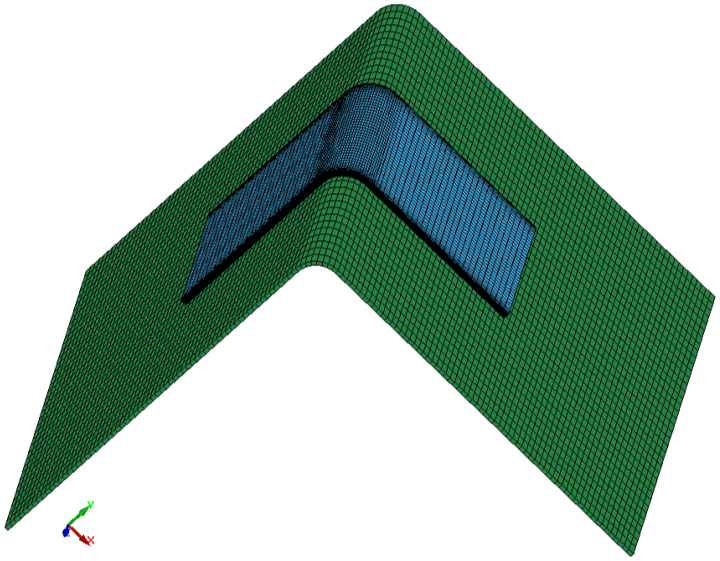

Figure 3.7: FE model simulating the steel tool and composite assembly.

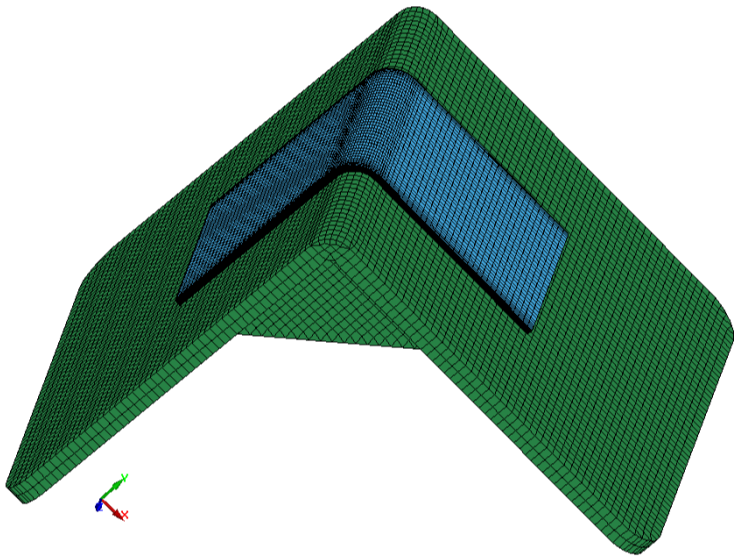

Figure 3.8: FE model simulating the titanium tool and composite assembly.

The material properties of the 3D printed titanium and conventional steel tools commonly used in aerospace applications are shown in Table 3.1.

Property	Titanium	Steel
Modulus of Elasticity $[GPa]$	113.8	200
Density $[kg/m^3]$	4430	7800
Poisson's Ratio $[-]$	0.342	0.24
Specific Heat Capacity$[J/kgK]$	526.3	460
Thermal Conductivity $[W/mK]$	6.7	24.9
Coefficient of Thermal Expansion $[°C^{-1}]$	9.2	10.8

Table 3.1: Material properties of the two tools.

For defining the tools' materials mechanical and thermal properties in LS-DYNA, models MAT_ELASTIC, MAT_THERMAL_ISOTROPIC as well as MAT_THERMAL_EXPANSION were used respectively, with the last one to be utilized in order to consider the thermal stains to the total strain calculation.

Similarly, for the composite material MAT_ORTHOTROPIC_THERMAL_CURING and MAT_THERMAL_ORTHOTROPIC LS-DYNA material models were used, with the first one described in a previous section. The material card details are available in Appendix A. The CTE values were assumed constant for the composite, while the CSC were given as a function of the DoC. For validation puproses the CSC and DoC values through simulation time are exported as history variables in LS-DYNA. It's important to note that the glassy state properties of the composite were utilized for the linear elastic material model. This decision was made because the higher CTE and CSC of the composite in its rubbery state would likely result in greater distortion values. By using the glassy properties, the aim was to prevent an overestimation of distortion.

3.2.2.2 FE mesh, Ply and Laminate Definitions

Regarding the FE meshing methods used, it is noteworthy that although shell elements are often used in analysis of solidified composite components, they are not ideal for simulating residual stress and PIDs of composite parts under curing. This happens as shell elements, usually based on CLT, cannot properly model the material behaviour in the thickness direction, which has a significant role in contact analysis [21]. Therefore, solid elements were utilized in this thesis study.

The deformation of the composite part, taking place as a combination of thermal expansion and chemical shrinkage phenomena, is the subject of study in this thesis. Using ANSYS ACP software each ply of thickness 0.19 mm was modeled with one solid element though its thickness [19]. To properly define each ply, a local coordinate system used by introducing the longitudinal and transverse directions. By this method, it is ensured that the fibre direction is assigned along the length of the composite plane and not the width, as well as that the normal direction is always perpendicular to the surface, irrespective of the type of surface, being flat or curved.

For describing the orthotropic laminate behavior for each of the four lay-ups, SOLID_ORTHO element type was used. By this option, the different properties of each ply in the laminate was described, as the proper material orientation was defined in the elements of each ply by introducing its fiber angle direction. An example is given in Figure 3.9, for an element belonging in a 90° ply of the quasi-isotropic laminate model.

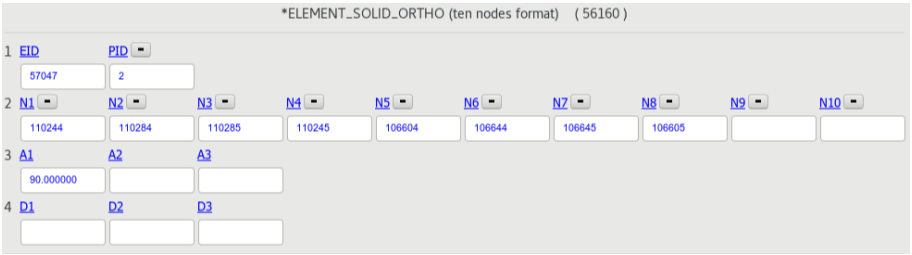

Figure 3.9: Composite element defined using SOLID_ORTHO option, with fibre orientation to 90°.

In addition, the corner region of the L-shaped structure was discretised using a more dense mesh, as can be noticed in Figure 3.6. During the mesh design, great attention was paid to the maximum limit for the element aspect ratio that corresponds to the ratio between the in-plane and through-thickness element dimensions. For too high element aspect ratio values, calculation stability can be affected [17]. Therefore, hexahedra linear 8-node fully-integrated elements (8 Gauss points) were used, with LS-DYNA element formulation (ELFORM) set to -2 in order to capture the the behavior of the elements with higher aspect ratio in the corner area. Overall, the composite part was simulated with a mesh of 56160 elements.

As for the tools, they undergo deformation of expansion and contraction under the

temperature changes, with no complex phenomena contributing to their deformation. Since the tools deformation is not a subject of study in this thesis, a rather dense mesh was utilized for these parts, using the conventional SOLID element type for the isotropic materials. However, it was important to use a finer mesh in the tools' corner region as well, since a coarsely meshed corner would result in element penetrations between the tool and part elements of the region. Therefore, similar to the composite, linear 8-node fully-integrated elements utilized for the hex-shaped dominated mesh with element formulation set to -2. The total number of elements in the titanium tool-composite model is 69854, while the corresponding one for the steel tool-composite model is 59608.

3.2.2.3 Thermal Loading and Vacuum Pressure

The loads applied on the components are of two types. Thermal loads were applied on the tool and composite resulting from the temperature cycle of the curing oven. In addition, mechanical loads were acting on the composite applied as the action of the vacuum bagging pressure.

The temperature cycle and the vacuum pressure are described in Figure 3.10 expressed with the unit system used in LS-DYNA. Divided into three steps, the initial temperature of the assembly was 20 ° C. Heating till the curing temperature within 3600 s, there was isothermal hold of the structure at 180 ° C till time 10800 s. Last, the cool down of the structure to room temperature was complete at 14400 s, remaining at this temperature till the end of the simulation time at 14500 s.

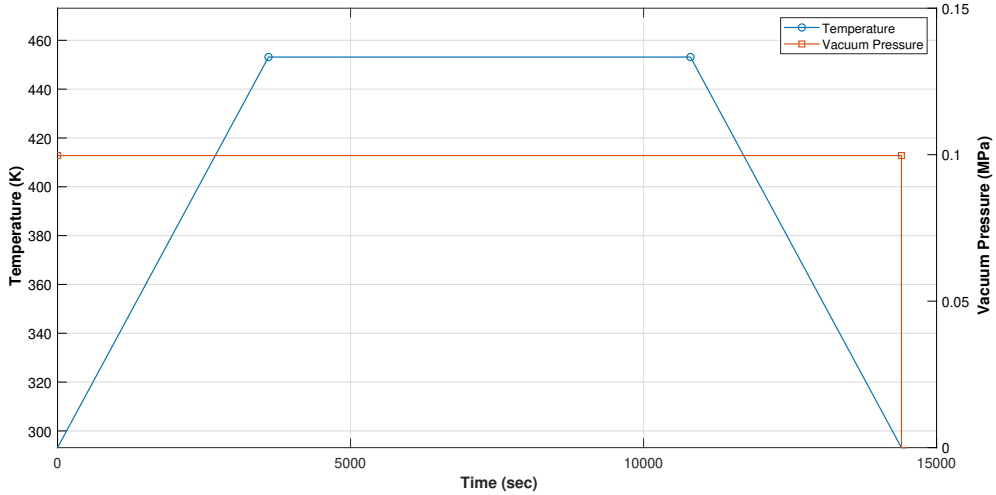

Figure 3.10: Temperature and pressure loads acting during curing.

Following the assumption of uniform temperature field on the surfaces of the tool-composite assembly exposed in the air of the oven, the temperature cycle was applied to the nodes of these surfaces using BOUNDARY_SPC_SET option. According to literature [9] in order to reduce computational cost, an assumption could be made for parts with a thickness of less than 3 mm, considering them to have a homogeneous

temperature field. In our case with a composite part approximating this thickness, a heat transfer analysis was employed prior to the mechanical one analysis in order to capture temperature gradients in the composite that can its distortion.

The vacuum bag pressure was applied on the top and side faces of the composite part that were in contact with the vacuum bag. Measuring an approximate pressure of 3 *mbar* during the manufacturing of L-shaped parts, a constant magnitude of 997 *mbar* was assumed to be active during cure and was removed when demolding started. It is noted that this pressure is expressed in terms of gauge and not absolute pressure.

3.2.2.4 Boundary Conditions and Contact Modeling

In this subsection, the description of the FE model simulating only the composite part is perform first, a model in which the fixed boundary conditions approach was used as described in the theory section. Then the description of the two models including the tool-composite assembly follows, simulations where the interaction between the parts is defined using the contact boundary condition approach.

For the simplified simulation, where the composite part was only modeled, the interaction with the tool was replaced by a mechanical boundary condition. Specifically, the nodes in the bottom surface of the composite that would interact with the tool, as shown in Figure 3.11, are fixed in x,y, and z transnational degrees of freedom. This assumption is performed to examine the accuracy of the fixed mechanical boundary condition that is often utilized in literature [30].

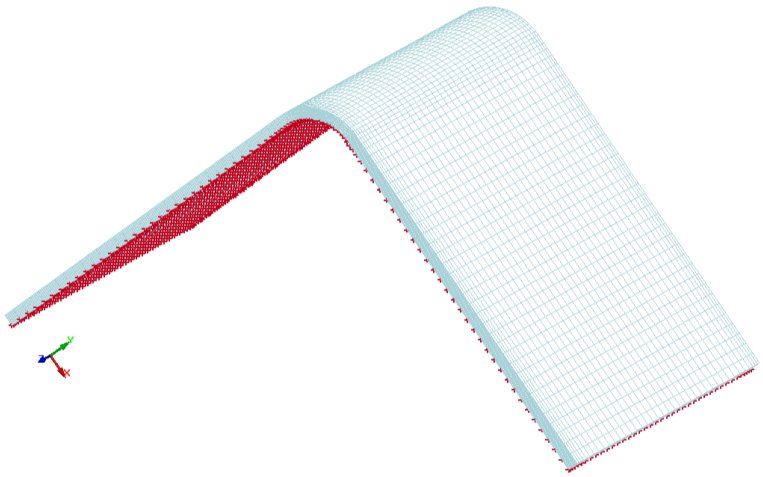

Figure 3.11: Fixed mechanical boundary condition during curing for the FE model including only the composite part.

The aforementioned boundary condition was active until the curing cycle was complete and deactivated at demolding. When demolding starts, boundary conditions as shown in Figure 3.12 were applied at three nodes in order to suppress rigid body motion of the composite, allowing it though to freely deform. In particular, node

1 is fixed in all translational DoFs preventing the translation of the composite part in space. Node 2 is restrained in x and z translational DoFs to prevent the rotation of the part around y and z axes, while node 3 restrained in x translational DoF prevented the rotation of the part around y axis. It is noted here that, following the global coordinate system of Figure 3.12, y-axis corresponds to the fibre direction (longitudinal), z-axis to flange width direction (transverse), and x-axis to laminate thickness direction.

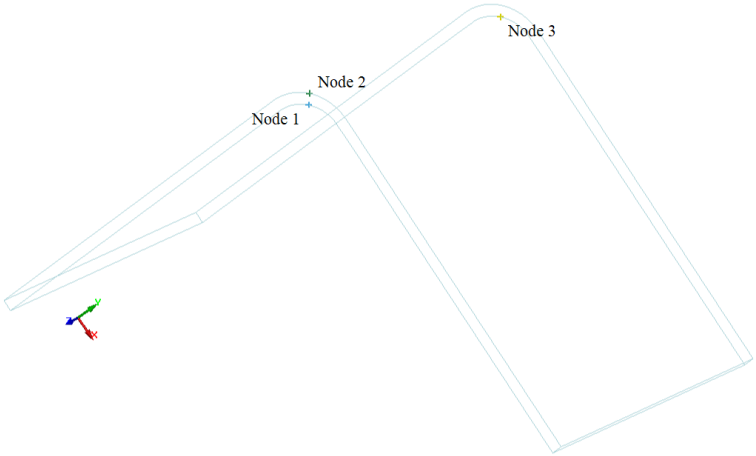

Figure 3.12: Boundary conditions applied to nodes 1 (blue), 2 (green) and 3 (yellow) to restraint rigid body motion of the composite during demolding phase.

For the FE models where both the tool and composite are simulated, the interaction between them is defined by the appropriate contact method. With the applied pressure constraining the L-shaped part to the tool during the curing, two contact approaches were examined and no other boundary condition was applied to the composite during curing. These are the CONTACT_AUTOMATIC_SURFACE_TO_SURFACE_MORTAR_TIED and CONTACT_AUTOMATIC_SURFACE_TO_SURFACE_MORTAR options. The first one is examined in order to be compared with the fixed mechanical boundary conditions applied in the case of the standalone composite model. The 'tied' algorithm was employed in the normal direction of the tool-part interface to prevent the components penetrating each other, as well as in the tangential direction to represent a case of significantly high CoF. The second contact option is examined as a more realistic approach, since there is no actual restriction (glue or other mechanical connection) between the bottom surface of the composite and the tool. In this case, the contact condition between the composite part and the tool during curing is defined such that the nodes of the contacting surfaces are constrained in the normal direction, while sliding along the surfaces is permitted with a specified CoF.

Elaborating on the selection of the aforementioned contact options, utilizing the AUTOMATIC_SURFACE_TO_SURFACE algorithm ensured that both surfaces in contact are checked for penetration to each other, although by using this option the computational cost was increased. The MORTAR algorithm was selected since

it is developed for implicit solver and recommended to use for implicit analysis [31].

Defining the parameters for the contact modeling as illustrated in Figure 3.13, the static CoF (FS) is a measure of the frictional force that must be overcome to initiate sliding between two surfaces. A constant FS was used and set equal to 0.3, value that is often used in literature [9, 28, 32]. For the dynamic CoF (FD) no relevant information was available. For the sliding contact case, FD was set using the empirical formula to the 0.8 of the value of FS, hence resulting to 0.24. For the 'tied' Mortar contact the dynamic value was set equal to the static, as recommended by the LS-DYNA manual [31]. The rest of the parameters shown in Figure 3.13 are set to the default value.

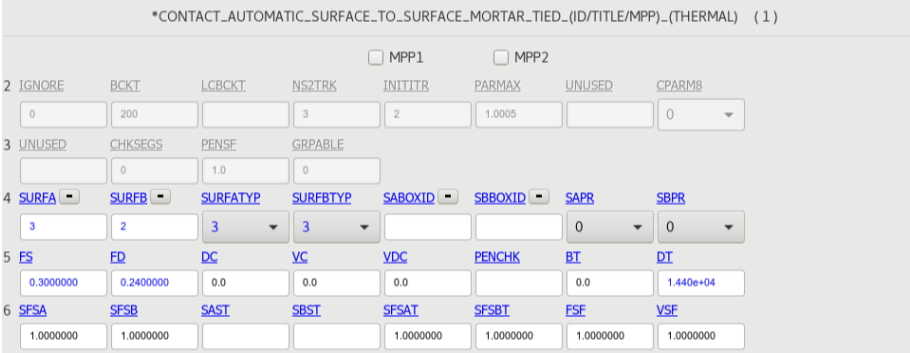

Figure 3.13: Definition of contact parameters in LS-DYNA.

As for the surfaces in contact defined by SURFA and SURFB fields, it is required by LS-DYNA that SURFA surface should be the surface with the softer material possessing also a finer mesh. Keeping this in mind, the composite surface has been selected as SURFA while the tool surface is set as SURFB, since the tool part is less deformable than the composite one. However, it must be noted that the assignment of the surfaces in contact in in SURFA and SURFB fields was not of importance in this model since AUTOMATIC_SURFACE_TO_SURFACE algorithm is used.

Similarly to the FE model of the composite part, the contact algorithm was active during curing and deactivated at demolding. When demolding starts, the boundary conditions described for Figure 3.11 were applied at the three nodes in order to suppress rigid body motion of the composite.

The boundary conditions acting on the tools are applied to suppress the rigid body motion of the tool. As depicted in Figure 3.14 for the titanium tool, the left edge was restricted in horizontal and vertical directions according to the local coordinate system shown. Two nodes at the ends of the same edge were fully restrained to ensure symmetric expansion of the tool along its length, while artificially restricting any expansion in the width direction. In the right edge, the nodes were restricted in the vertical direction only so as to allow the free expansion of the tool. Similar boundary conditions were used in the FE model with the steel tool. By these conditions, apart from preventing the rigid body motion of the tool, symmetry was induced in the way the tool could expand with thermal changes.

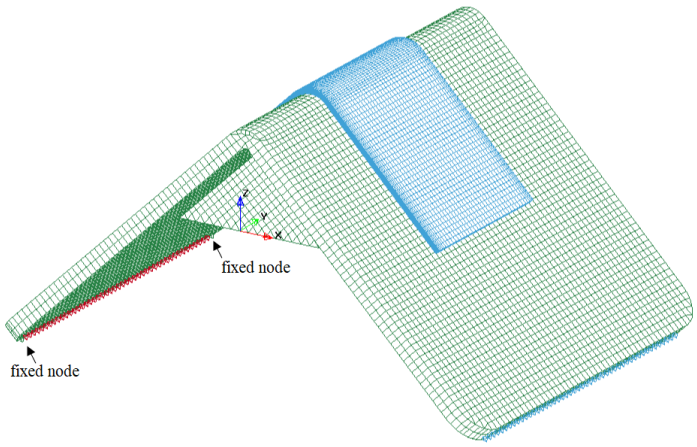

Figure 3.14: Boundary conditions applied to left edge nodes (red) with two fixed nodes as well as in right edge nodes (blue), to restraint rigid body motion of the tool.

3.2.2.5 Simulation and Analysis Settings

As described previously, thermo-mechanical analyses were needed to simulate the composite curing process and evaluate the PIDs. For this problem the fields of temperature and displacement were coupled, with the transient thermal analysis to be performed prior to the mechanical one, using a constant time step size of 10 s, as suggested from LS-DYNA Manual [31] for this type of analysis. After the temperature field was identified at each time step, the mechanical analysis was performed with the same constant time step size, in order to calculate of the distortion of the structure.

Overall, the FE simulations were performed using an implicit solver for the static problem with a small-strain assumption, with the contact definition introducing non-linearity in the models of tool-composite assembly. The simulations were solved using parallel method utilizing 12 CPU cores.

3.2.3 Measurement Methods for Spring-in and Warpage

Before the results of the FE models are discussed, it is important to demonstrate the measurement techniques used to experimentally and numerically evaluate spring-in and warpage of the composite parts. The methods utilized for validating the FE models in terms of spring-in and warpage are explained, along with those used to analyze the effects of tool material and composite lay-up sequence on PIDs. It is important to note that in all simulations, the evaluation of the shape distortions took place in the bottom surface region of the composite part by consistently selecting the same nodes for taking measurements in each simulation.

For the experimental spring-in angle measurement performed by RISE, the best-fit plane was first estimated for the surfaces of each of the eight components. This was achieved by approximating the plane that minimized the overall distance between

the scanned surface points, using specialized software for accurate fitting. Once the best-fit plane was determined, the angle between the scanned surface and this plane was measured at three different cross-sections along the width of the surface. An average spring-in angle can be then computed based on these three measurements.

For the numerical spring-in measurement, a selection of four nodes was performed in the edge of the laminate along its length direction, as depicted in Figure 3.15. With each node pair to define a line in one initially flat flange of the composite, the change of the angle between the two lines is computed, starting from 90° at the beginning of the simulation.

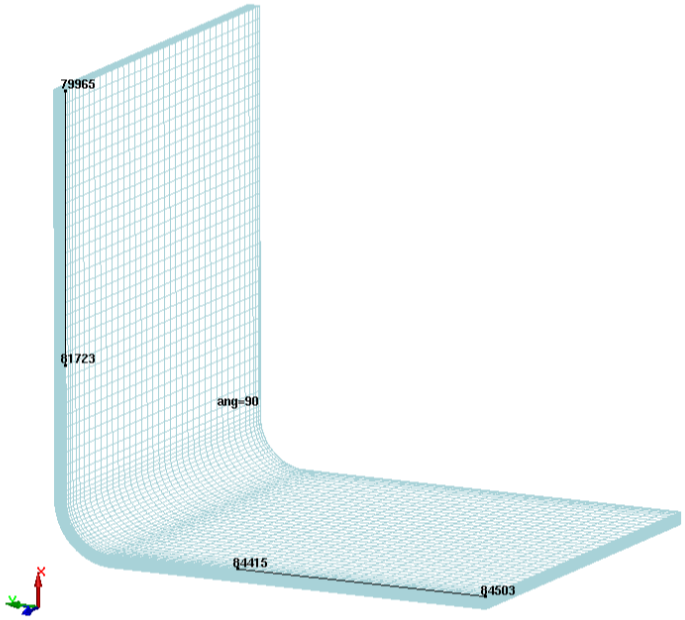

Figure 3.15: Spring-in evaluation in composite during post-processing by measuring the angle between four selected nodes.

It should be noted that, to maintain consistency with the experimental spring-in measurements, the angle was also measured at the middle cross-section of the flange width and at the opposite edge, using the same methodology. However, since the variations in these values were negligible, only the measurement from one edge of the flange was considered, as shown in Figure 3.15.

For the FE model validation in terms of spring-in, the numerical spring-in angle was compared with the average spring-in angle measured experimentally for each component. In analyzing the results concerning the effects of tool material and composite lay-up on spring-in, the estimated angles were grouped and compared to identify trends and draw conclusions.

Regarding warpage, the FE model validation took place by a surface topology method as performed by RISE. By this method, the numerically predicted surface,

which was defined by the displacements of the composite's surface nodes at the final simulation time step, was aligned and compared with the 3D-scanned surface for each manufactured specimen. Considering the experimental results as the accurate ones, the overall geometric deviation (topology misalignment) between simulations and the scanned results was then evaluated.

In analyzing the effects of tool material and composite lay-up on warpage, the displacements of the scanned surface points in the through-thickness direction were measured quantitatively, using a best-fit plane as a reference. As a next step, the warpage measurements were taken along the middle cross-sections of the 100 mm x 100 mm flange surface in both the width and length directions, as shown in Figures 3.16 and 3.17, respectively.

It must be highlighted that the numerical measurement methods play a significant role in the validation of the FE models. The aforementioned methods are approaches that are commonly used in literature, simplified for the purposes of this master thesis. Their integrity is questioned, since the complex distortion phenomena lead to difficulties in evaluating spring-in angle and warpage independently from each other. A key example is the spring-in computation where the angle is evaluated between the two straight lines shown in Figure 3.15, although it is known that the lines are in reality not totally straight due to warpage.

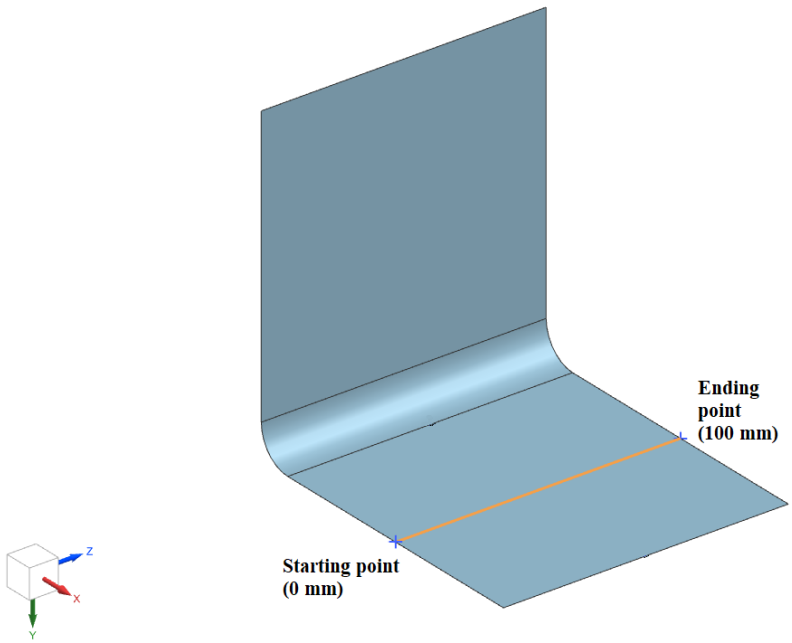

Figure 3.16: Cross-section where warpage across composite flange width was estimated.

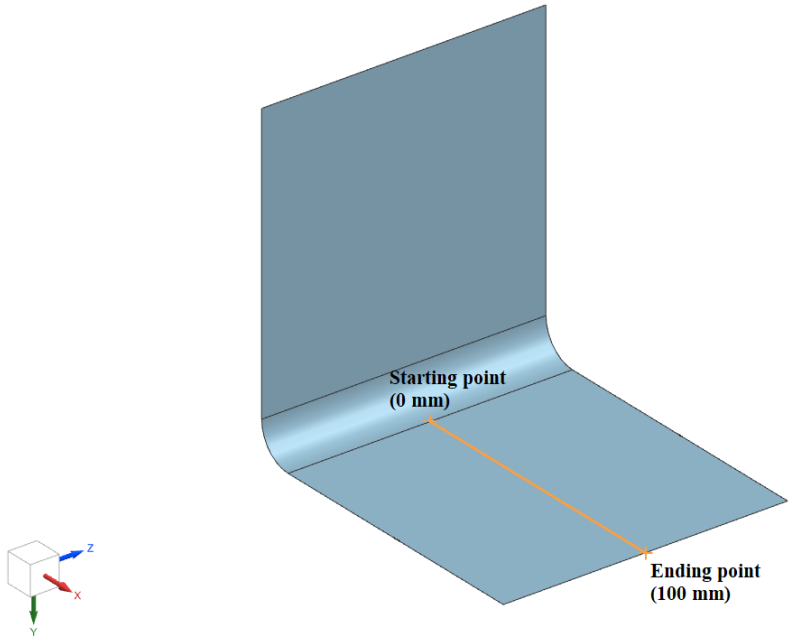

Figure 3.17: Cross-section where warpage across composite flange length was estimated.

4

Results and Discussion

In this section the validation of numerical results is presented using the distortion measurements from the manufactured components. Overall, twenty-four simulations were performed, as three boundary or contact conditions were examined for the eight manufactured components. As discussed in previous sections, these were: an FE model in which only the composite was simulated while the tool was replaced by a fixed mechanical boundary condition, as well as two FE models simulating both the composite and the tool parts using the 'tied' Mortar and 'sliding' Mortar contact algorithms for the interface respectively.

Following the FE model validation, the analysis of the results was conducted to examine the effect of the tool material on the development of spring-in and warpage distortions. A study was also performed to investigate the influence of the composite lay-up on these distortions.

4.1 FE Model Validation

The experimental validation of the FE models that were built-up in terms of this master thesis was carried out using the L-shaped composite parts manufactured.

The three FE models of fixed mechanical boundary conditions (BC), 'tied' contact (MORTAR_TIED) and sliding contact (MORTAR), were first validated by comparing the numerically measured spring-in angle to the one measured experimentally, as shown in Table 4.1.

Titanium - UD 0°	Spring-in (°)
BC	0.504
MORTAR_TIED	0.504
MORTAR	0.504
Exp.	**0.937**

Steel - UD 0°	Spring-in (°)
BC	0.504
MORTAR_TIED	0.504
MORTAR	0.504
Exp.	**0.083**

Titanium - UD 90°	Spring-in (°)
BC	0.001
MORTAR_TIED	0.001
MORTAR	0.001
Exp.	**0.31**

Steel - UD 90°	Spring-in (°)
BC	0.001
MORTAR_TIED	0.001
MORTAR	0.001
Exp.	**-1.13**

Titanium - Quasi-Isotropic	Spring-in (°)
BC	0.6427
MORTAR_TIED	0.6427
MORTAR	0.6427
Exp.	**1.523**

Steel - Quasi-Isotropic	Spring-in (°)
BC	0.635
MORTAR_TIED	0.635
MORTAR	0.635
Exp.	**0.233**

Titanium - Asymmetric	Spring-in (°)
BC	-1.336
MORTAR_TIED	-1.336
MORTAR	-1.336
Exp.	**0.623**

Steel - Asymmetric	Spring-in (°)
BC	-1.174
MORTAR_TIED	-1.174
MORTAR	-1.174
Exp.	**-0.657**

Table 4.1: Spring-in angle numerical and experimental measurements.

It should be noted that a positive angle indicates spring-in, where the angle of the composite part decreases after curing, while a negative angle indicates spring-out, with the angle increasing after curing.

As an initial observation, the three FE models result to the same spring-in angle value for each of the eight components, which is expected given the purely linear elastic material model used. This model does not account for the loading history or visco-elastic behavior, suggesting that more advanced material models capable of capturing the actual material behavior could influence the spring-in predictions. Comparing to results of previous studies [9, 25], both the fixed BC and tool-part

contact simulation predict rather realistically the average spring-in angle. However, for most of the test conducted in [9, 25], the tool-part contact simulation results to a more accurate spring-in angle compared to the fixed BC which can underestimate the value.

Identifying the experimental spring-in value as the exact one, the percentage error between the absolute numerical and experimental spring-in values is calculated using the formula:

$$Error\ (\%) = \frac{\mid \Delta\theta^{num} \mid \ - \ \mid \Delta\theta^{exp} \mid}{\mid \Delta\theta^{exp} \mid} \ \times \ 100 \tag{4.1}$$

The results are reported in Table 4.2. In all cases, the computed percentage error is major. A positive error indicates that the simulation overestimates the spring-in angle compared to the experimental results, while a negative error reflects an underestimation. These significant variations highlight the limitations of the numerical model in capturing the exact spring-in behavior of the manufactured specimens.

Component	Error (%)
Titanium - UD 0°	-46.38
Titanium - UD 90°	-99.67
Titanium - Quasi-Isotropic	-57.78
Titanium - Asymmetric	+114.61
Steel - UD 0°	+507.22
Steel - UD 90°	-99.91
Steel - Quasi-Isotropic	+172.53
Steel - Asymmetric	+78.69

Table 4.2: Error as percentage difference between the absolute values of numerical and the experimental spring-in measurement.

For validating the FE model against the warpage distortion measurements, a comparison between the node topology and the 3D-scanned surface is presented for each component in Figures 4.1 to 4.8. The color bar in these figures represents the resultant displacement, showing the overall geometric deviation of the simulations from the scanned results. The MORTAR simulation model was selected for validation after comparing the three numerical predictions for each component. Since all simulations produced similar distortion results, only the MORTAR model was chosen as the basis for FE validation in order to minimize additional costs associated with the node topology method.

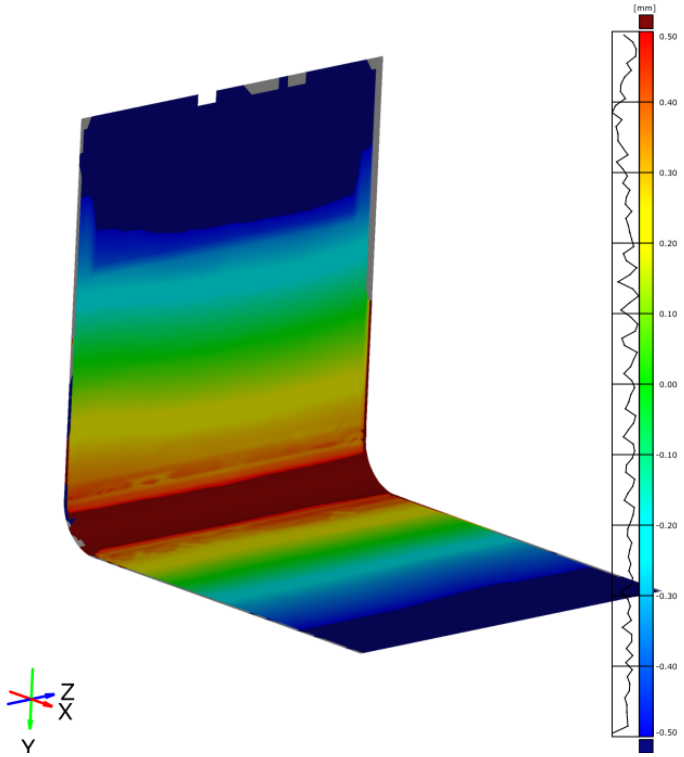

Figure 4.1: Nodes topology (MORTAR) aligned and compared to 3D-scanned L-profile analysis, Titanium - UD 0°.

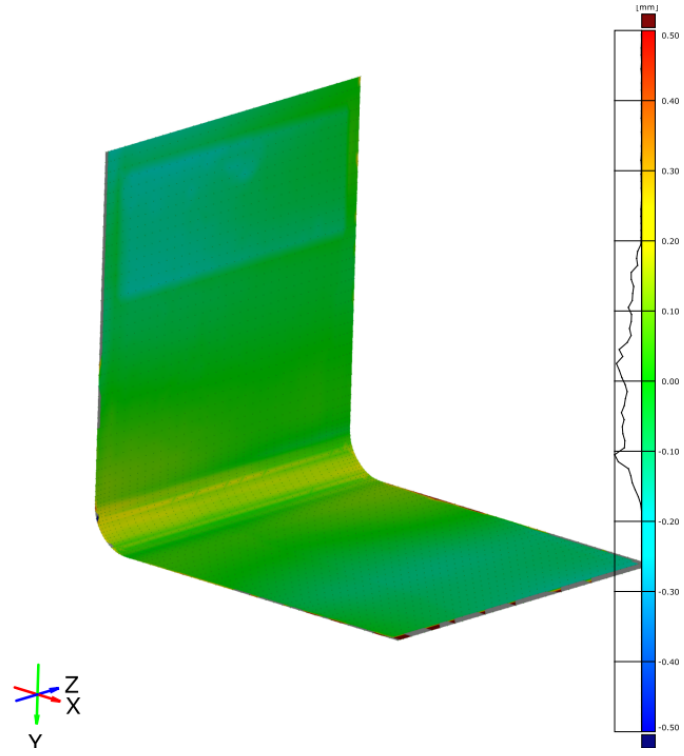

Figure 4.2: Nodes topology (MORTAR) aligned and compared to 3D-scanned L-profile analysis, Titanium - UD 90°.

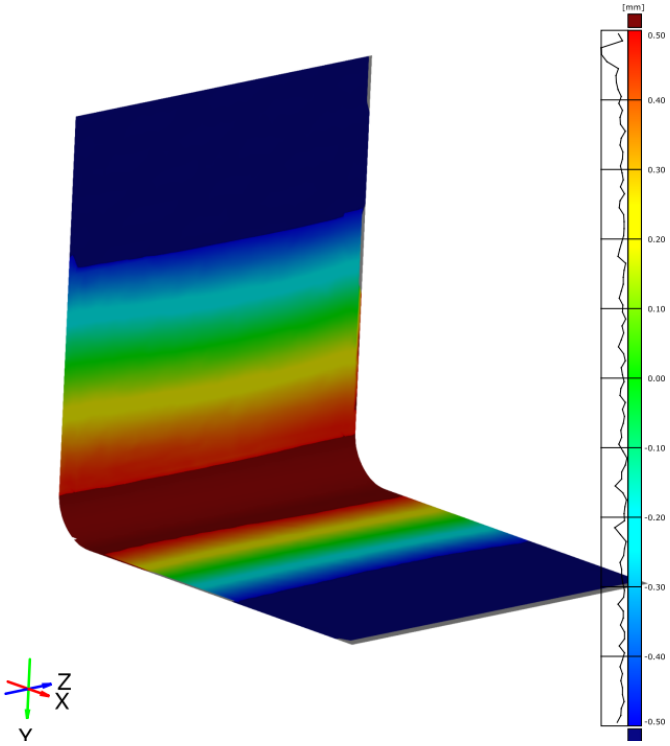

Figure 4.3: Nodes topology (MORTAR) aligned and compared to 3D-scanned L-profile analysis, Titanium - Quasi-Isotropic.

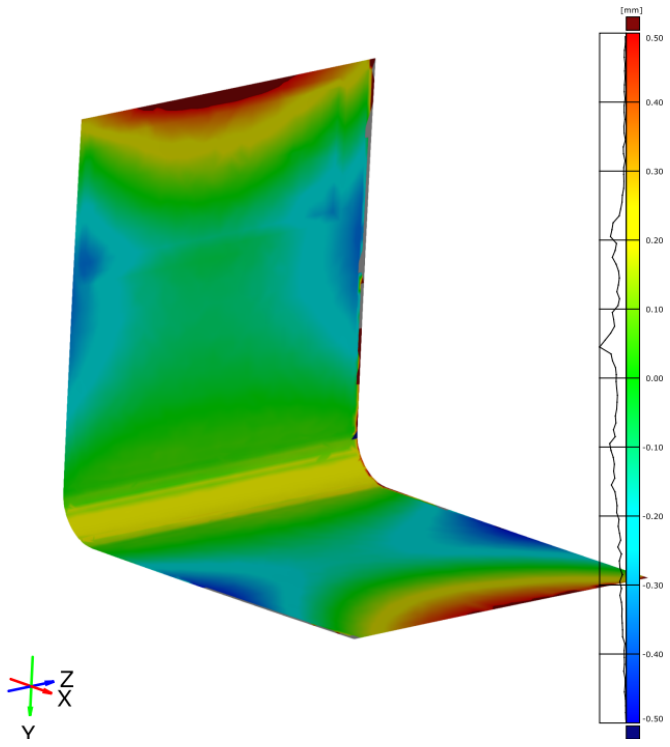

Figure 4.4: Nodes topology (MORTAR) aligned and compared to 3D-scanned L-profile analysis, Titanium - Asymmetric.

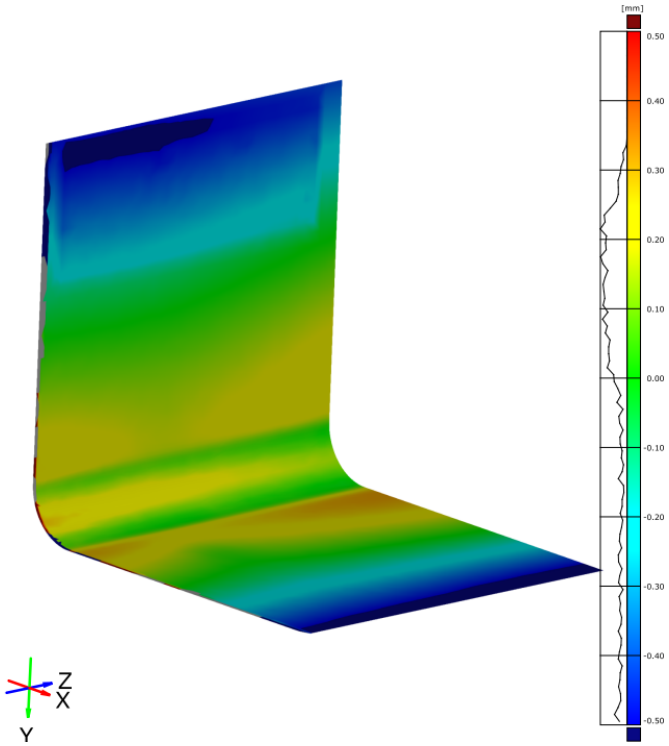

Figure 4.5: Nodes topology (MORTAR) aligned and compared to 3D-scanned L-profile analysis, Steel - UD 0°.

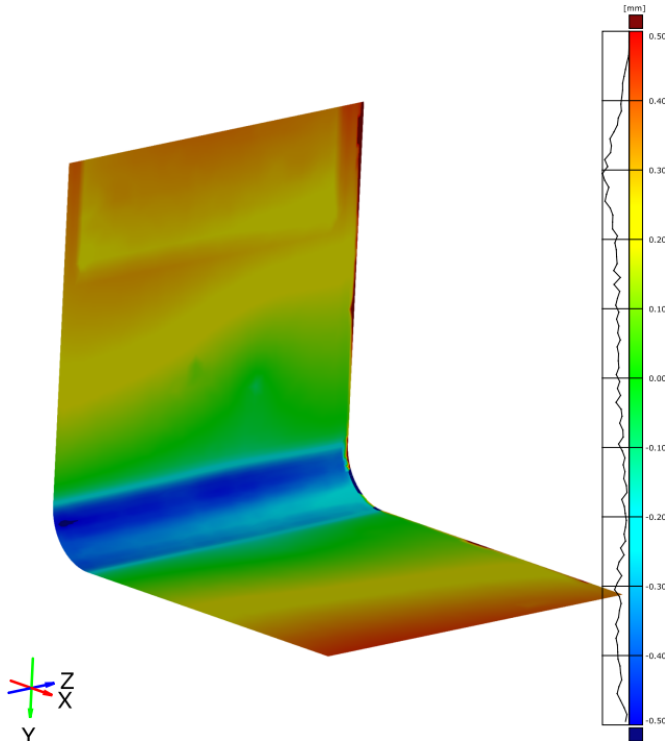

Figure 4.6: Nodes topology (MORTAR) aligned and compared to 3D-scanned L-profile analysis, Steel - UD 90°.

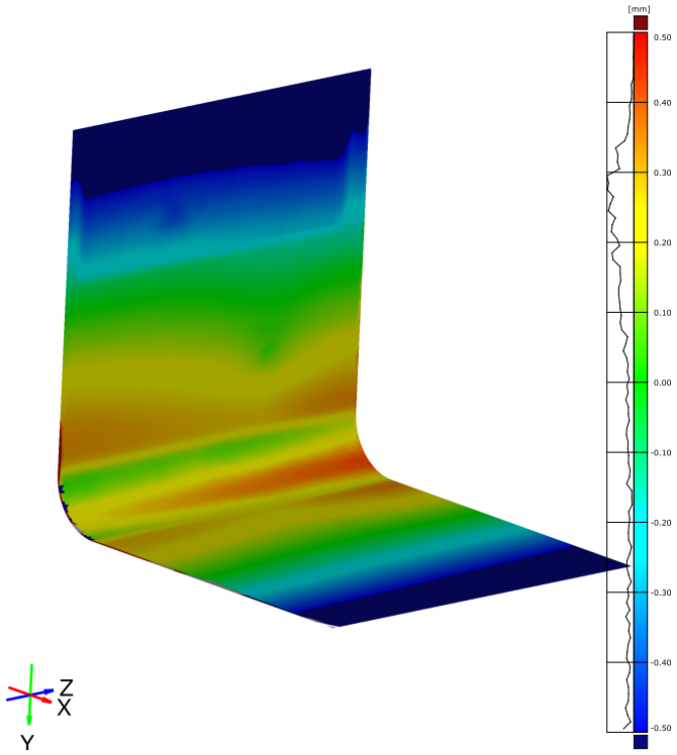

Figure 4.7: Nodes topology (MORTAR) aligned and compared to 3D-scanned L-profile analysis, Steel - Quasi-Isotropic.

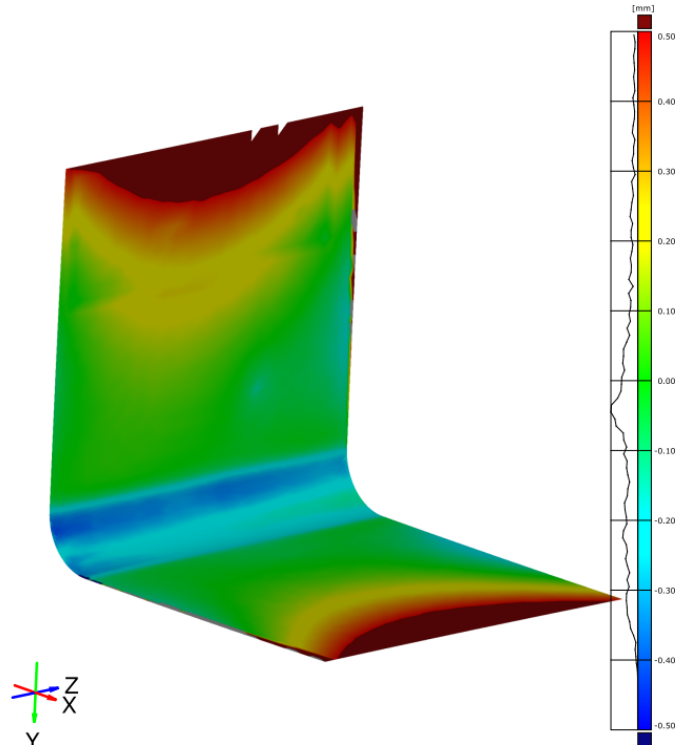

Figure 4.8: Nodes topology (MORTAR) aligned and compared to 3D-scanned L-profile analysis, Steel - Asymmetric.

For components manufactured using the titanium tool, Figures 4.1 and 4.3 show that the predicted warpage for both the 0° UD laminate and the quasi-isotropic laminate deviates significantly from the experimental results. In contrast, better alignment is observed in Figures 4.2 and 4.4 and for the 90° UD laminate and the asymmetric laminate, respectively. Notably, for the UD 90° case, the numerical predictions are highly accurate, differing from the experimental measurements by only a small margin of ± 0.1 mm. For the asymmetric lay-up case the deviation is significant only in the composite's edges, especially along the width direction.

A similar trend is observed for the components manufactured with a steel tool, with predictions for the UD 0° and quasi-isotropic cases to present the most significant deviation from experimental results, as shown in Figures 4.5 and 4.7. Comparing Figures 4.1 and 4.5, as well as 4.3 and 4.7, reveals similarities in misalignment predictions, with the largest discrepancies occurring at the edges along the width direction. According to Figure 4.6, deformation predictions for the UD laminate with 90° plies show an accuracy within ± 0.4 mm compared to the experimental measurements. Similar to the titanium case, the asymmetric lay-up FE model for steel tool predicted deformation that deviates significantly from the experimental one along its edges in the width direction, as illustrated in Figure 4.8.

Overall, the prediction error (topology misalignment) is quite significant across most of the components. Notably, the highest errors occur in the regions where the spring-in measurements are taken. Given also the significant deviation between the numerical and experimental spring-in values, as shown in Table 4.2, the developed FE models can not be considered efficiently validated and 'be trusted' in providing accurate predictions for the process-induced spring-in and warpage of L-shaped composite parts.

4.2 Analysis of Spring-in and Warpage Results

4.2.1 Effect of Tool Material Selection

The effect of tool material on the induced spring-in angle is examined first. As concluded in the previous section, the FE models are not sufficiently validated; therefore, only the experimental results are used for the analysis. However, the ability of the numerical models to capture trends in spring-in estimation, relative to the experimental data, is also examined. To aid in visualization and comparison, the experimentally and numerically measured spring-in values are presented in Figures 4.9 and 4.10, grouped by the tool used.

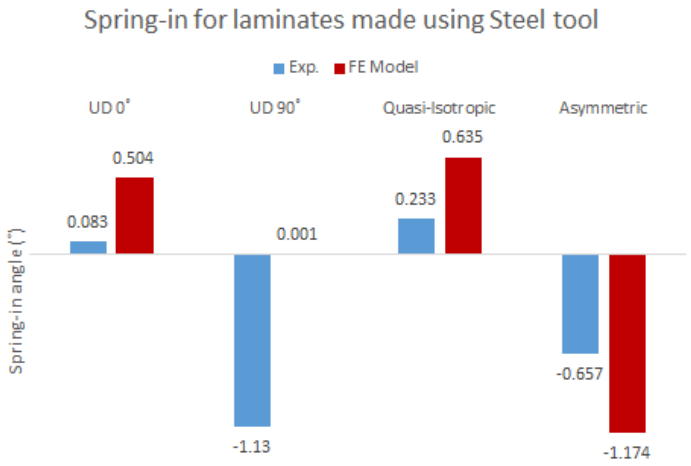

Figure 4.9: Experimentally measured spring-in angles for composites manufactured using steel tool.

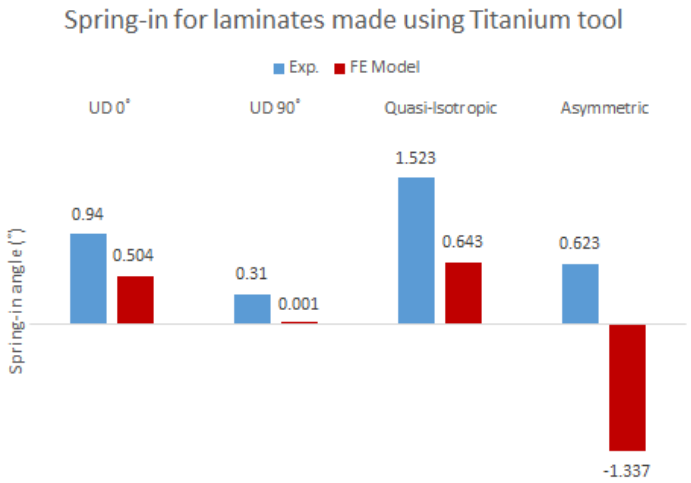

Figure 4.10: Experimentally measured spring-in angles for composites manufactured using titanium tool.

Comparing the two figures for each lay-up using the experimental measurements in terms of spring-in magnitude, the titanium tool results in a greater spring-in angle than the steel tool for UD 0° and quasi-isotropic lay-ups. In contrast, the steel tool produces a larger spring-in for UD 90° and asymmetric lay-ups. Based on these observations, a definitive conclusion cannot be drawn regarding which tool consistently leads to the highest spring-in angle.

As for the spring-in angles predicted by the FE models, the simulation results for the UD laminates are identical for both tools, with only minor differences observed in the quasi-isotropic and asymmetric cases. This indicates that the FE models do not effectively capture the influence of the tool material on spring-in behavior.

The effect of tool material on warpage distortion across the flange width and length directions is also studied. Distortion measurements for all eight manufactured components are available in Appendix B. Figures 4.11 to 4.14 illustrate the warpage in both directions for each lay-up, using the methods described in Figures 3.16 and 3.17 from a previous section. Unlike the spring-in results, the numerical warpage data are not included in the following Figures, as a quantitative comparison between the FE model and experimental results is not advisable, as explained in Appendix B.

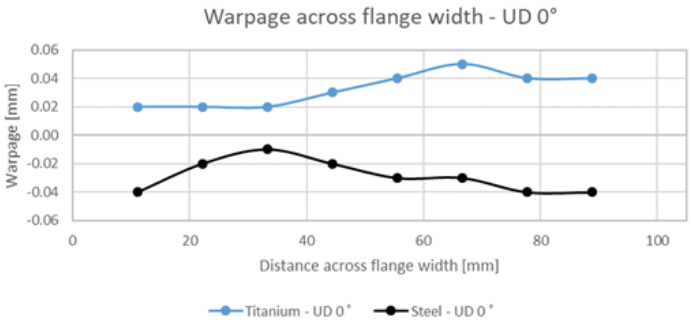

(a)

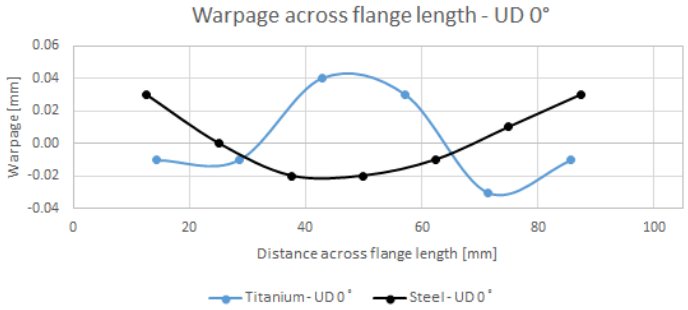

(b)

Figure 4.11: Warpage across flange (a) width and (b) length using experimental results, comparison between steel and titanium tools for $[0]_{16}$.

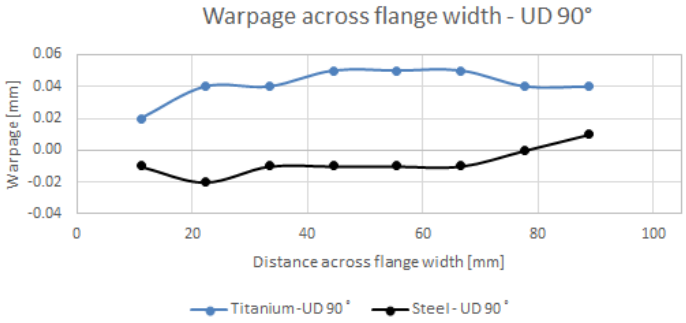

(a)

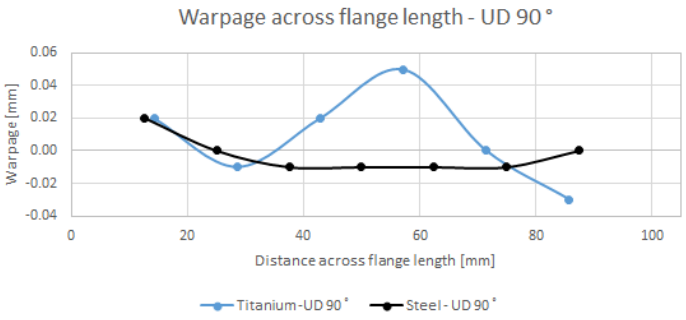

(b)

Figure 4.12: Warpage across flange (a) width and (b) length using experimental results, comparison between steel and titanium tools for $[90]_{16}$.

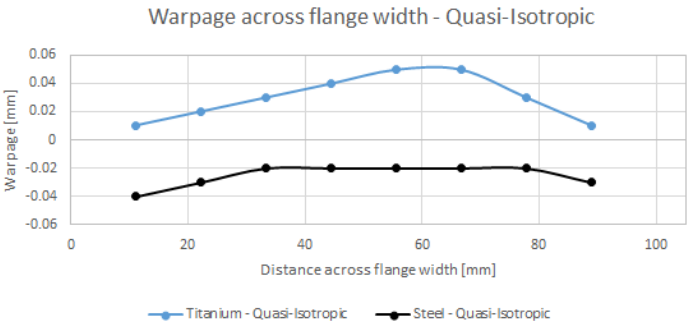

(a)

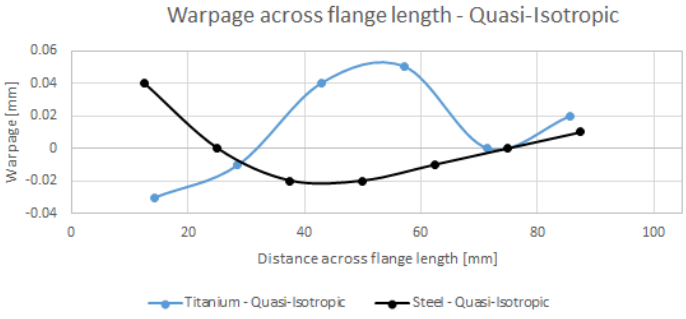

(b)

Figure 4.13: Warpage across flange (a) width and (b) length using experimental results, comparison between steel and titanium tools for $[0/\pm 45/90/0/\pm 45/90]_S$.

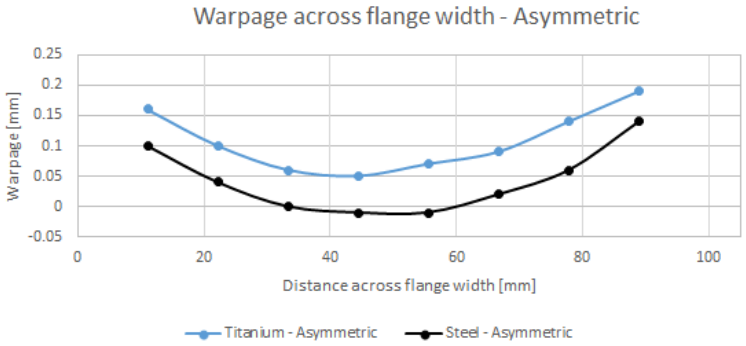

(a)

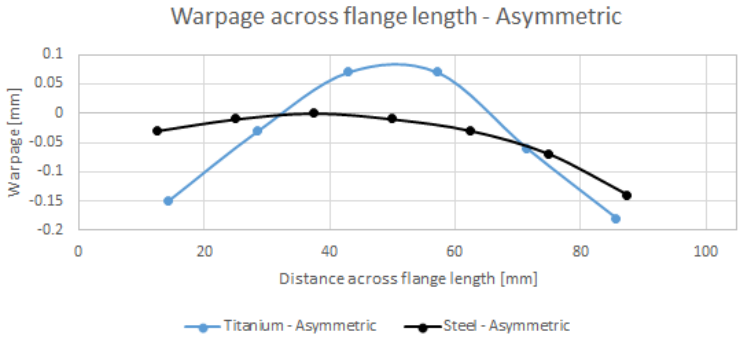

(b)

Figure 4.14: Warpage across flange (a) width and (b) length using experimental results, comparison between steel and titanium tools for $[0/\pm 45/90/0/\mp 45/90]_2$.

The experimental results for warpage measured as deviation from best-fit plane of each manufactured component reveal that, for all lay-ups, the titanium tool results in more significant deviation from the initially flat plane in both width and length direction. In addition, it could be noticed that for all lay-ups the deviations from a flat surface are higher (more abnormal distortions) across length direction than in width direction.

4.2.2 Effect of Composite Lay-up Selection

A similar analysis is conducted to examine the effect of composite lay-up in the induced spring-in angle, using Figures 4.9 and 4.10.

From the experimental results in Figure 4.9, the UD 90° laminate exhibits the largest spring-in magnitude for the steel tool, followed by the asymmetric, quasi-isotropic, and UD 0° laminates. In the case of the titanium tool, the quasi-isotropic laminate shows the largest spring-in, followed by the UD 0°, asymmetric, and UD 90° laminates. No definitive conclusion can be drawn from these results regarding a consistent trend.

As previously discussed, the FE simulations predict the same spring-in values regardless of the tool used. According to the simulations, the largest spring-in occurs in the asymmetric lay-up, followed by the quasi-isotropic, UD 0°, and UD 90° laminates. Once again, the FE models fail to accurately capture the spring-in trends

observed in the experimental results.

The effect of lay-up sequence is also studied for the induced warpage distortion across the flange width and length direction. Considering the experimental measurements of the deviation from best-fit planes as presented for each component in Appendix B, Figures 4.15 and 4.16 report the warpage in the two directions for four different laminates manufactured with steel and titanium material tool respectively.

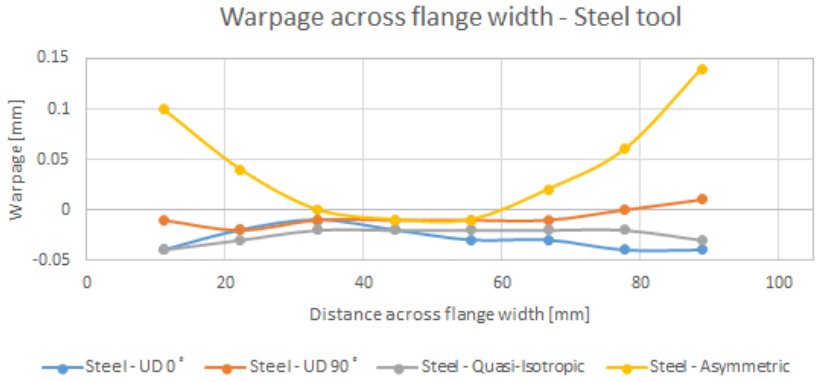

(a)

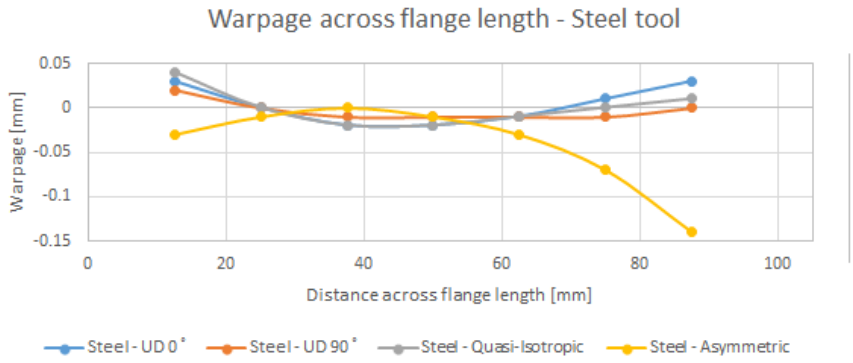

(b)

Figure 4.15: Warpage across flange (a) width and (b) length using experimental results, comparison between four different lay-ups manufactured using steel tool.

(a)

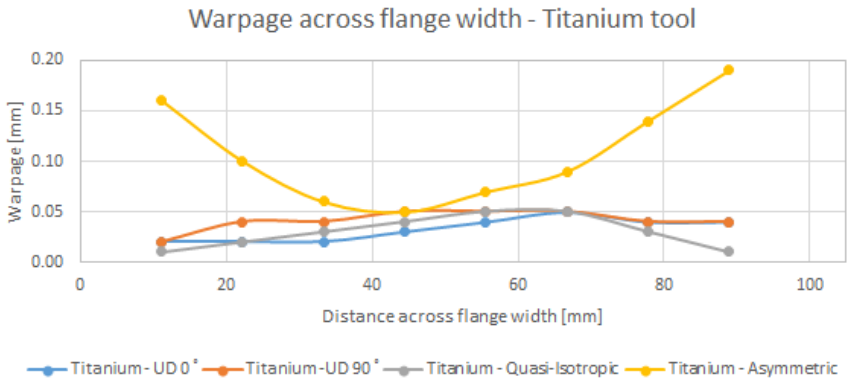

(b)

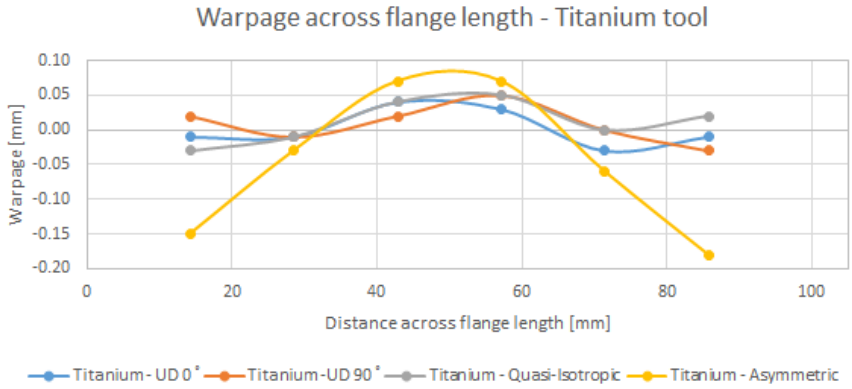

Figure 4.16: Warpage across flange (a) width and (b) length using experimental results, comparison between four different lay-ups manufactured using titanium tool.

It is obvious that the asymmetric laminate presents the significantly higher warpage distortion than the rest of the laminates in width as well as in length flange direction, for both steel and titanium cases. According to Figures 4.15 and 4.16 (a), the UD of 0° plies laminate appears to have slightly larger geometric deviations than the quasi-isotropic one, while the UD of 90° plies laminate presents the smallest deviations from flatness. This observation is not clear in Figure 4.16 (b) where, apart from the asymmetric case, the three rest laminates present approximately the same deviation magnitudes.

The different warpage results among the laminates, can be attributed to the fact that different lay-ups produce different bending stiffness matrices (D). This variation results in different stress distributions through the composite's thickness when subjected to the same tool-part interfacial shear stress, thereby leading to different bending moments and warpage [1, 5].

5
Conclusion

5.1 Key Findings

The main findings of this master thesis project can be concluded and related to the main goals of the project.

The findings of this study reveal that the simplified linear elastic material model, which does not account for thermal loading history and visco-elastic behavior, is inadequate for capturing the tool effect. This conclusion is reinforced by the parametric studies discussed in Appendix C. Since under these conditions the fixed mechanical boundary conditions, 'tied' and sliding Mortar contact algorithms predict similar spring-in values, the tool-part contact simulation becomes ineffective. The results indicate that a more accurate material model is needed for the composite to accurately assess the effect of the tool. In addition, when implementing such an FE model and validating it effectively, further research may be required to provide a more detailed representation of the tool-composite interface and refine the parameters defining the contact between the components.

Analysing the effect of the tool material on the experimental measurements, no definitive conclusion can be drawn regarding which tool material induces larger spring-in angles. The same uncertainty applies to the influence of the lay-up sequence on the spring-in angle. Regarding warpage, the titanium tool tends to induce more significant deviations from the initially flat composite surface compared to the steel tool. In addition, asymmetric laminates tend to present significantly higher warpage than the UD 0°, quasi-isotropic and UD 90° laminates. Since quasi-isotropic and zero-dominated quasi-isotropic laminates find the more applications in aerospace industry, the design of symmetric and balanced laminates to avoid the coupling of the bending and twisting distortions of the laminate is highlighted.

5.2 Recommendations for Future Research

Regarding the proper FE model validation, the implementation of more efficient methods to numerically measure spring-in and warpage is recommended in order to identify the FE simulations developed in this work as a precise tool for accurate spring-in and warpage prediction. The new methods should consider the effect of laminate warpage affecting the spring-in angle measurement. In particular, the flanges where the angle measurements are taken are not flat as initially were but become curved due to warpage. As for the topology misalignment method that is used for validation in terms of warpage, the definition of a criterion to quantitatively assess the deviation of the numerical results from the experimental ones is proposed. For instance, this could be described by a scalar value indicating the percentage of the numerically predicted surface (given by node topology) that fits the experimental one, within a given accuracy range. In addition, it is highlighted that this topology validation method involves comparing the manufactured composite surface with the nodal surface obtained from a single simulation. This process can be resource-intensive, as each adjustment to an FE model parameter requires a new comparison with updated simulation results. Therefore, it is recommended to prioritize FE validation by first comparing the scalar numerical and experimental spring-in results. Once this initial validation is achieved, further FE validation can proceed by focusing on warpage analysis. Lastly, repeating the manufacturing of each specimen under the same lay-up and tooling conditions is recommended, in order to examine whether the PID values obtained by the numerical simulations fall within the variability range of the measurements made on manufactured L-shaped laminates.

With the aim to improve the FE models, the simulation parameters that can lead to a realistic prediction for spring-in and warpage distortion for each case need to be detected. First and foremost, to effectively capture the composite's response PIDs throughout the curing cycle, it is suggested that the future work should be focused in the use of a more complicated but accurate material model for simulating the curing of the composite prepreg in LS-DYNA. The use of a UMAT considering the thermo-visco-elastic phenomena is suggested, in which the elastic moduli vary with temprature, DoC as well as with time. It is also significant to refine of the composite's CTE values in order to better match the ones of the material used for experiments. The values used in this study were based on existing data from similar previous studies, as specific data were not available at the time of this research. Consequently, these sources were utilized to complete the necessary simulations.

In addition, considering the tool-composite simulation as a the most realistic approach, further research could be contacted in determining the appropriate contact algorithm for this application in LS-DYNA. The use of a thermal contact condition involving the heat transfer across surfaces should be considered, and the relative parameters need to be defined such as the thermal conductance of the surfaces in contact. In addition, further research may be needed to precisely calibrate and determine contact surface parameters such as the initial fluid friction shear strength at a zero DoC. Another area for improvement involves refining the CoF to better

reflect the actual experimental process, since the current values are based on previous studies in literature. Regarding the latter one, another approach could be the investigation of cure-dependent CoF. However, according to findings of study [9] the use of the cure-dependent CoF was found to have minimal impact on the results while significantly increasing computational costs and, therefore, a constant CoF could be assumed throughout the analysis without reducing simulation accuracy.

The identification of the simulation parameters having a significant effect in PID development is important in order to avoid determining the unnecessary ones. Regarding this aspect, some guidelines can be provided based on the results of this master thesis. Previous studies on flat laminates [3] indicate that part deflection can be significantly reduced by an appropriate material selection, as well as by a change in the specific heat of the tooling. For the purposes of the current study, the conduction of a sensitivity analysis is recommended focusing on the investigation of the effect of the tool material CTE, the CoF between the tool and the composite, as well as the effect of the applied cooling rate during curing on the PID development.

Lastly, it would be beneficial to re-evaluate the assumptions made in this study. In the developed FE simulations, the cure cycle used in the experiment was applied to all nodes the model. For a more accurate simulation, convection boundary conditions should be applied for the heat transfer process from the air in the curing oven to the composite part, considering also the effect of the vacuum bag material on the part. Moreover, lay-up variations should be accounted such as effect of varying thickness in the manufactured specimens.

It is highlighted that in order to ensure that results from coupon L-profile samples can be reliably applied to larger parts with more complex geometry, significant extrinsic parameters (manufacturing conditions and technique, composite and tool material, bagging arrangement) have to be identical through all manufacturing processes. Thus, identifying and exploring the possible impact of all significant mechanisms and factors that influence PIDs is essential for accurately predicting and mitigating the total distortion in L-shaped prepreg laminates.

Bibliography

[1] E. Zappino, N. Zobeiry, M. Petrolo, R. Vaziri, E. Carrera, A. Poursartip, Analysis of process-induced deformations and residual stresses in curved composite parts considering transverse shear stress and thickness stretching, *Composite Structures*, Volume 241, 2020, 112057, ISSN 0263-8223.

[2] A. Ding, S. Li, J. Sun, J. Wang, L. Zu, A thermo-viscoelastic model of process-induced residual stresses in composite structures with considering thermal dependence, *Composite Structures*, Volume 136, 2016, Pages 34-43, ISSN 0263-8223.

[3] D. Stefaniak, E. Kappel, T. Spröwitz, C. Hühne, Experimental identification of process parameters inducing warpage of autoclave-processed CFRP parts, *Composites Part A: Applied Science and Manufacturing*, Volume 43, Issue 7, 2012, Pages 1081-1091, ISSN 1359-835X.

[4] E. Kappel, D. Stefaniak, T. Spröwitz, C. Hühne, A semi-analytical simulation strategy and its application to warpage of autoclave-processed CFRP parts, *Composites Part A: Applied Science and Manufacturing*, Volume 42, Issue 12,2011, Pages 1985-1994, ISSN 1359-835X.

[5] Z. Yuan, Y. Wang, X. Peng, J. Wang, S. Wei, An analytical model on through-thickness stresses and warpage of composite laminates due to tool-part interaction, *Composites Part B: Engineering*, Volume 91, 2016.

[6] A. Ding, J. Wang, A. Ni, S. Li, A new analytical solution for cure-induced spring-in of L-shaped composite parts, *Composites Science and Technology*, Volume 171, 2019, Pages 1-12, ISSN 0266-3538.

[7] G. Twigg, A. Poursartip, G. Fernlund, Tool–part interaction in composites processing. Part I: experimental investigation and analytical model, *Composites Part A: Applied Science and Manufacturing*, Volume 35, Issue 1, 2004, Pages 121-133, ISSN 1359-835X.

[8] G. Twigg, A. Poursartip, G. Fernlund, Tool–part interaction in composites processing. Part II: numerical modelling, *Composites Part A: Applied Science and Manufacturing*, Volume 35, Issue 1, 2004, Pages 135-141, ISSN 1359-835X.

[9] N. Traiforos, M. Matveev, D. Chronopoulos, T. Turner, Spring-in of composite L-shape specimens: An experimental and numerical investigation, *Composite Structures*, Volume 310, 2023, 116772, ISSN 0263-8223.

[10] S. Saseendran, Process Modelling of Prepreg Composite Materials: FE Modelling of Warpage and Distortion during Curing, Master's Thesis, TU Braunschweig, 2012.

[11] M.R. Wisnom, M. Gigliotti, N. Ersoy, M. Campbell, K.D. Potter, Mechanisms generating residual stresses and distortion during manufacture of poly-

mer–matrix composite structures, *Composites Part A: Applied Science and Manufacturing*, Volume 37, Issue 4, 2006, Pages 522-529, ISSN 1359-835X.

[12] L. Mezeix, A. Seman, M.N. Mohd Nazreen, Y. Aminanda, A. Rivai, B. Castanié, P. Olivier, K.M. Ali, Spring-back simulation of unidirectional carbon/epoxy flat laminate composite manufactured through autoclave process, *Composite Structures*, Volume 124, 2015.

[13] N. Ersoy, K. Potter, M.R. Wisnom, M.J. Clegg, An experimental method to study the frictional processes during composites manufacturing, *Composites Part A: Applied Science and Manufacturing*, Volume 36, Issue 11, 2005, Pages 1536-1544, ISSN 1359-835X.

[14] E. Kappel, D. Stefaniak, G. Fernlund, Predicting process-induced distortions in composite manufacturing – A pheno-numerical simulation strategy, *Composite Structures*, Volume 120, 2015, Pages 98-106, ISSN 0263-8223.

[15] Q. Wang, T. Li, X. Yang, K. Wang, B. Wang, M. Ren, Prediction and compensation of process-induced distortions for L-shaped 3D woven composites, *Composites Part A: Applied Science and Manufacturing*, Volume 141, 2021, 106211, ISSN 1359-835X.

[16] T. Garstka, Separation of Process Induced Distortions in Curved Composite Laminates, Doctoral Thesis, University of Bristol, 2005.

[17] C. Bellini, L. Sorrentino, W. Polini, A. Corrado, Spring-in analysis of CFRP thin laminates: numerical and experimental results, *Composite Structures*, Volume 173, 2017, Pages 17-24.

[18] A. Ding, S. Li, J. Wang, A. Ni, A new analytical solution for spring-in of curved composite parts, *Composites Science and Technology*, Volume 142, 2017, Pages 30-40, ISSN 0266-3538.

[19] K. Çınar, N. Ersoy, Effect of fibre wrinkling to the spring-in behaviour of L-shaped composite materials, *Composites Part A: Applied Science and Manufacturing*, Volume 69, 2015, Pages 105-114, ISSN 1359-835X.

[20] G. Zhang, J. Wang, A. Ni, H. Hu, A. Ding, S. Li, Process-induced deformation of L-shaped variable-stiffness composite structures during cure, *Composite Structures*, Volume 230, 2019, 111461, ISSN 0263-8223.

[21] X. Zeng, J. Raghavan, Role of tool-part interaction in process-induced warpage of autoclave-manufactured composite structures, *Composites Part A: Applied Science and Manufacturing*, Volume 41, Issue 9, 2010, Pages 1174-1183, ISSN 1359-835X.

[22] C. Schoenholz, N. Zobeiry, Investigating the impacts of processing variability on tool-part interaction for interply-toughened aerospace composites using a novel shear technique, *Composites Part A: Applied Science and Manufacturing*, Volume 178, 2024, 107973, ISSN 1359-835X.

[23] S. Minakuchi, S. Niwa, K. Takagaki, N. Takeda, Composite cure simulation scheme fully integrating internal strain measurement, *Composites Part A: Applied Science and Manufacturing*, Volume 84, 2016, Pages 53-63, ISSN 1359-835X.

[24] A.A. Johnston, An integrated model of the development of process-induced deformation in autoclave processing of composite structures, Ph.D. thesis, University of British Columbia, 1997.

[25] J.M. Svanberg, Predictions of Manufacturing Induced Shape Distortions, Doctoral Thesis, Luleå University of Technology, 2002.

[26] S. Saseendran, D. Berglund, J. Varna, Viscoelastic model with complex rheological behavior (VisCoR): incremental formulation, *Advanced Manufacturing: Polymer & Composites Science*, Volume 6, Issue 1, 2020, Pages 1-16.

[27] *LS-DYNA Keyword User's Manual Volume II: Material Models*, Livermore Software Technology (LST), An Ansys Company, 2020.

[28] K. Çınar, N. Ersoy, 3D finite element model for predicting manufacturing distortions of composite parts, *Journal of Composite Materials*, Volume 50, Issue 27, 2016, Pages 3791-3807.

[29] V. Kaushik, J. Raghavan, Experimental study of tool–part interaction during autoclave processing of thermoset polymer composite structures, *Composites Part A: Applied Science and Manufacturing*, Volume 41, Issue 9, 2010, Pages 1210-1218, ISSN 1359-835X.

[30] A. Osooly, Development and Implementation of Robust Large Deformation and Contact Mechanics Capabilities in Process Modelling of Composites, Doctoral Thesis, The University of British Columbia, 2008.

[31] *LS-DYNA Keyword User's Manual Volume I*, Livermore Software Technology (LST), An Ansys Company, 2020.

[32] L. Khoun, R. de Oliveira, V. Michaud, P. Hubert, Investigation of process-induced strains development by fibre Bragg grating sensors in resin transfer moulded composites, *Composites Part A: Applied Science and Manufacturing*, Volume 42, Issue 3, 2011, Pages 274-282, ISSN 1359-835X.

[33] M. Fiorina, A. Seman, B. Castanié, K.M. Ali, C. Schwob, L. Mezeix, Spring-in prediction for carbon/epoxy aerospace composite structure, *Composite Structures*, Volume 168, 2017.

[34] X. Cao, H. Tian, H. Dalir, Development of a new finite element simulation strategy for prediction of thermal and resin shrinkage deformations of composite parts during cure, In B.D. Davidson, M.W. Czabaj, J.G. Ratcliffe (Eds.), *Proceedings of the American Society for Composites – 31st Technical Conference, ASC 2016*, DEStech Publications Inc., 2016.

A

Appendix

LS-DYNA Material Cards for Composite

```
LS-DYNA keyword deck by LS-PrePost
$================ LS-DYNA Material model card (mid) ================================================
*MAT_ORTHOTROPIC_THERMAL_CURING_TITLE
linearly elastic, orthotropic material with orthotropic thermal expansion
Constant properties are used for Young's moduli (e), Poisson's ratio (pr), Shear moduli, and CTE (a)
$#     mid        ro        ea        eb        ec      prba      prca      prcb
         11.56500E-9  121500.0    6700.0    6700.0    0.0138    0.0138     0.369
$#     gab       gbc       gca        aa        ab        ac      aopt      macf
    3135.0    2447.0    3135.0 4.3000E-7-3.9200E-5-3.9200E-5                    1
$#      xp        yp        zp        a1        a2        a3
$#      v1        v2        v3        d1        d2        d3      beta       ref
                                                                          0
$#      k1        k2        c1        c2         m         n         r
1.300000E7       0.0   87870.0       0.0       1.0    1.0000     8.314
$#   lccha     lcchb     lcchc      lcaa      lcab      lcac
         4         5         6



*DEFINE_CURVE_TITLE
CSC given as a function of the DoC, direction a
$#    lcid      sidr       sfa       sfo      offa      offo    dattyp     lcint
         4         0       1.0       1.0       0.0       0.0         0         0
$#                a1                  o1
                0.0                 0.0
                0.4           1.2500E-6
                1.0           1.2000E-4
*DEFINE_CURVE_TITLE
CSC given as a function of the DoC, direction b
$#    lcid      sidr       sfa       sfo      offa      offo    dattyp     lcint
         5         0       1.0       1.0       0.0       0.0         0         0
$#                a1                  o1
                0.0                 0.0
                0.4              0.0074
                1.0              0.0065
*DEFINE_CURVE_TITLE
CSC given as a function of the DoC, direction c
$#    lcid      sidr       sfa       sfo      offa      offo    dattyp     lcint
         6         0       1.0       1.0       0.0       0.0         0         0
$#                a1                  o1
                0.0                 0.0
                0.4              0.0074
                1.0              0.0065
```

```
$================ LS-DYNA Thermal material card (tmid)============
$ thumat13 CFRP
*MAT_THERMAL_ORTHOTROPIC_TD_LC
$      tmid       tro      tgrlc    tgmult      aopt      tlat      hlat
$#     tmid       tro      tgrlc    tgmult      aopt      tlat      hlat
          11.56500E-9          0       0.0       0.0
$       lcc      lck1       lck2      lck3
$#      lcc      lck1       lck2      lck3   ilcchsv   ilckhsv    itghsv
          1         2          3         3
$#       xp        yp         zp        a1        a2        a3
        0.0       0.0        0.0       0.0       0.0       0.0
$#       d1        d2         d3
        0.0       0.0        0.0


*DEFINE_CURVE
$#    lcid      sidr       sfa       sfo      offa      offo    dattyp     lcint
         1         0       1.0       0.0       0.0       0.0         0         0
$        abcissa (x)        ordinate (y)
$#                a1                 o1
              -200.0    1.2000000000e+09
               773.0    1.2000000000e+09
*DEFINE_CURVE
$#    lcid      sidr       sfa       sfo      offa      offo    dattyp     lcint
         2         0       1.0       0.0       0.0       0.0         0         0
$        abcissa (x)        ordinate (y)
$#                a1                 o1
              -200.0               10.0
               773.0               10.0
*DEFINE_CURVE
$#    lcid      sidr       sfa       sfo      offa      offo    dattyp     lcint
         3         0       1.0       0.0       0.0       0.0         0         0
$        abcissa (x)        ordinate (y)
$#                a1                 o1
              -200.0                1.0
               773.0                1.0
```

B

Appendix

Experimental Measurements for Deviation from best-fit planes

The experimental measurement results presented in the following sections represent deviations in the manufactured laminate from best-fit planes, as measured by RISE. These deviations are distances perpendicular to each flange and are used to generate Figures 4.11 to 4.14 to show the effect of tool material on warpage, as well as Figures 4.15 and 4.16 to illustrate the effect of composite lay-up sequence on warpage.

Simulation results are provided to assess whether a similar deformation pattern (warpage) is captured compared to the experimental results. For simplicity, the simulations are based on analyses where only the laminate is modeled, using boundary conditions instead of contact, as all three FE models produced similar x-displacement responses for each component. It is important to note that the simulation results depict the magnitude of x-direction displacement at the final time step and should not be directly compared to the experimental distance deviation measurements. Instead, the x-displacement results should be visually compared to the corresponding experimental measurements specifically in the top flange region.

B.1 $[0]_{16}$ - Titanium tool

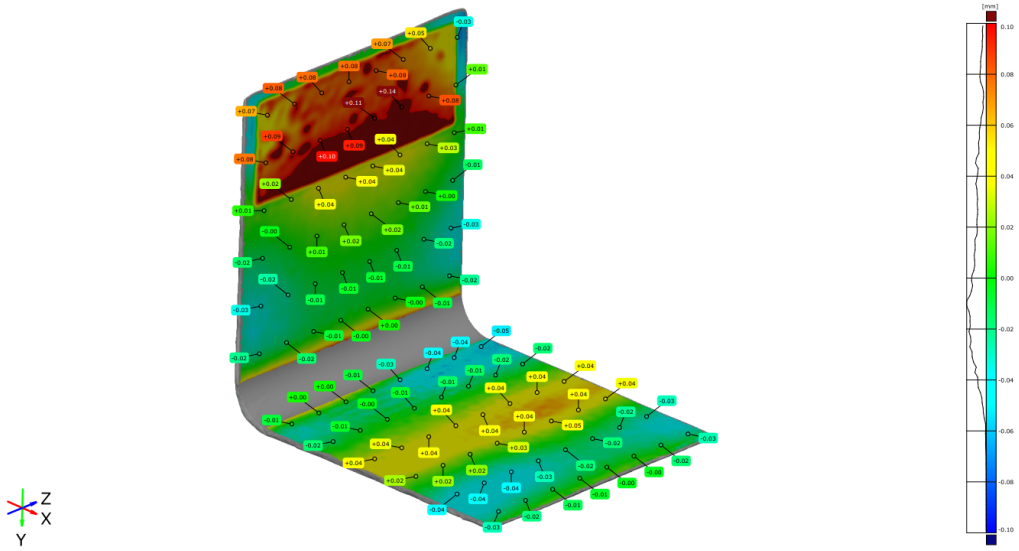

Figure B.1: Experimental measurement - Deviation to best-fit planes, $[0]_{16}$ using titanium tool.

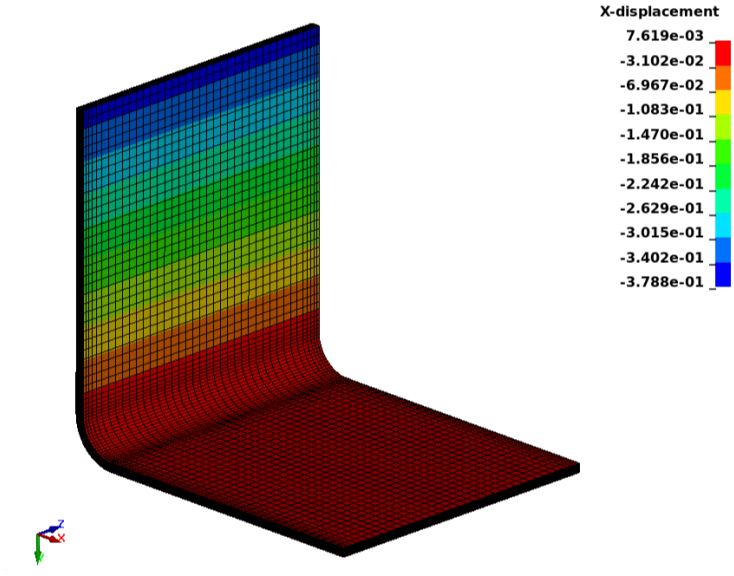

Figure B.2: Simulation result for X-displacement, $[0]_{16}$ using titanium tool.

B.2 $[90]_{16}$ - Titanium tool

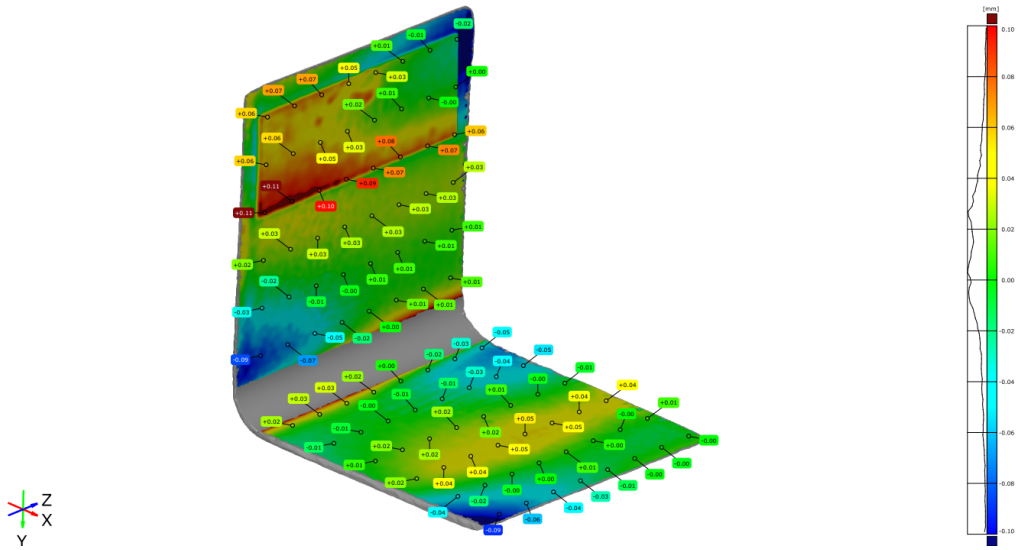

Figure B.3: Experimental measurement - Deviation to best-fit planes, $[90]_{16}$ using titanium tool.

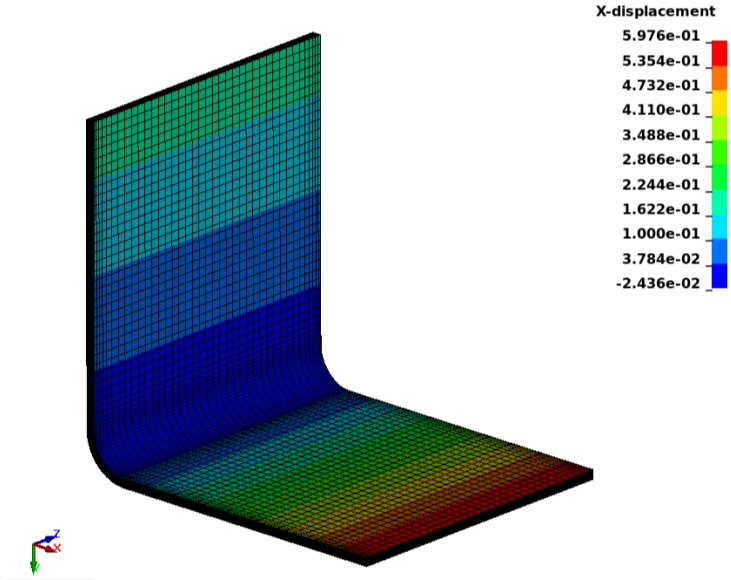

Figure B.4: Simulation result for X-displacement, $[90]_{16}$ using titanium tool.

B.3 $[0/\pm 45/90/0/\pm 45/90]_S$ - Titanium tool

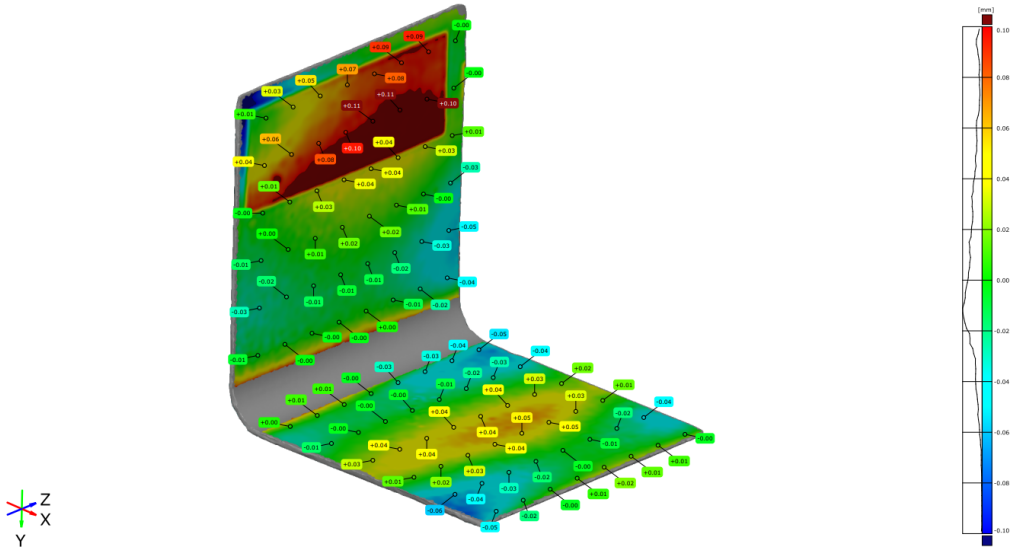

Figure B.5: Experimental measurement - Deviation to best-fit planes, $[0/\pm 45/90/0/\pm 45/90]_S$ using titanium tool.

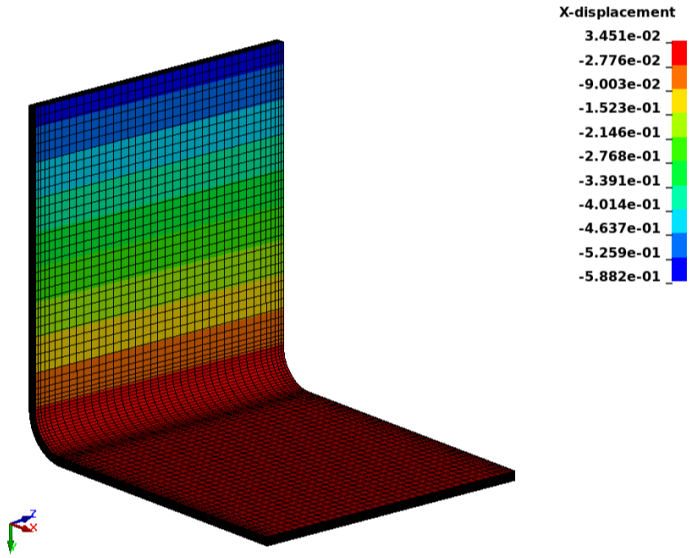

Figure B.6: Simulation result for X-displacement, $[0/\pm 45/90/0/\pm 45/90]_S$ using titanium tool.

B.4 $[0/\pm 45/90/0/\mp 45/90]_2$ - Titanium tool

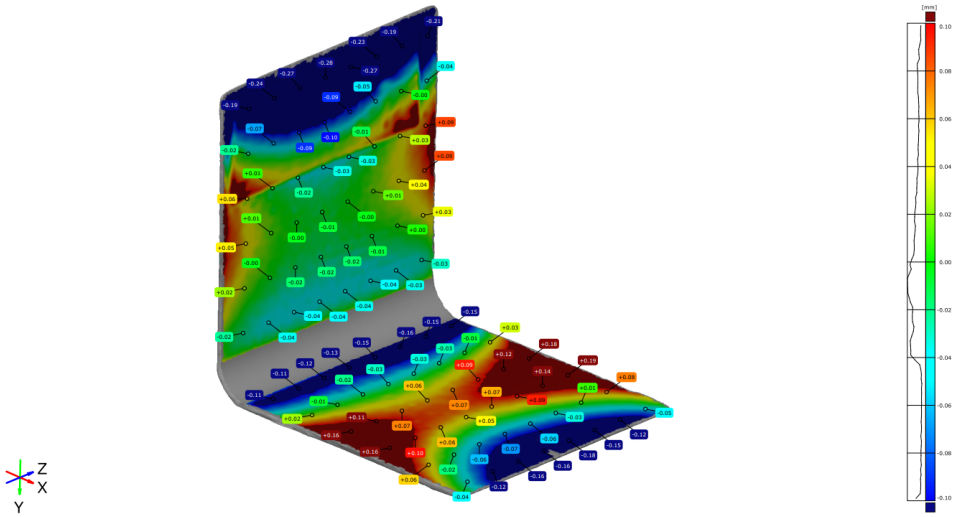

Figure B.7: Experimental measurement - Deviation to best-fit planes, $[0/\pm 45/90/0/\mp 45/90]_2$ using titanium tool.

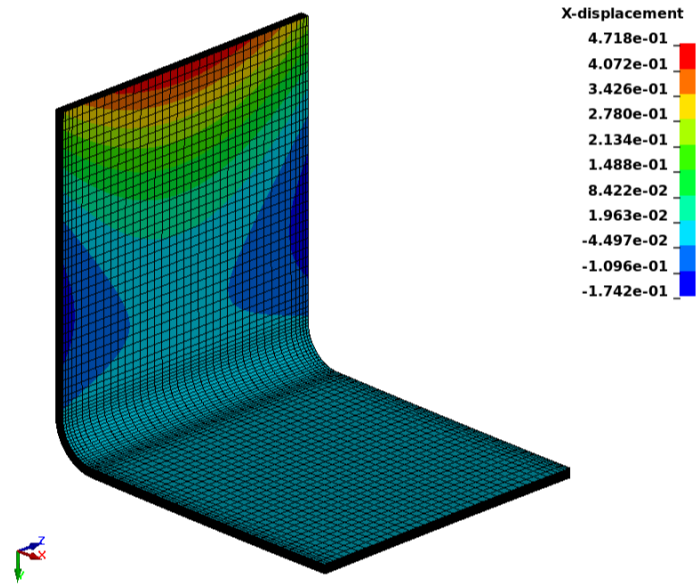

Figure B.8: Simulation result for X-displacement, $[0/\pm 45/90/0/\mp 45/90]_2$ using titanium tool.

B.5 $[0]_{16}$ - Steel tool

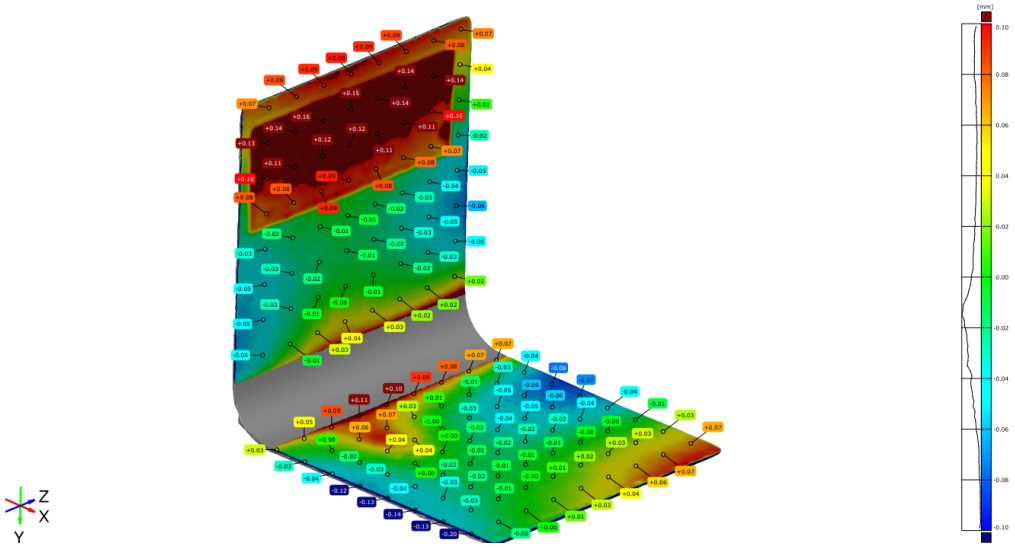

Figure B.9: Experimental measurement - Deviation to best-fit planes, $[0]_{16}$ using steel tool.

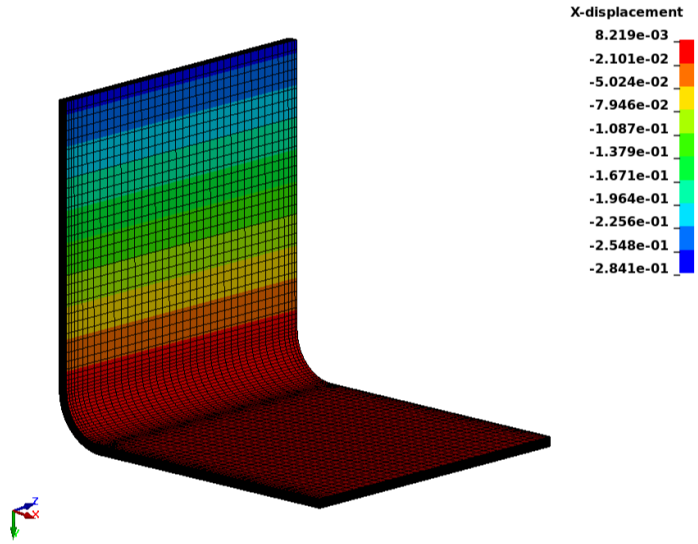

Figure B.10: Simulation result for X-displacement, $[0]_{16}$ using steel tool.

B.6 $[90]_{16}$ - Steel tool

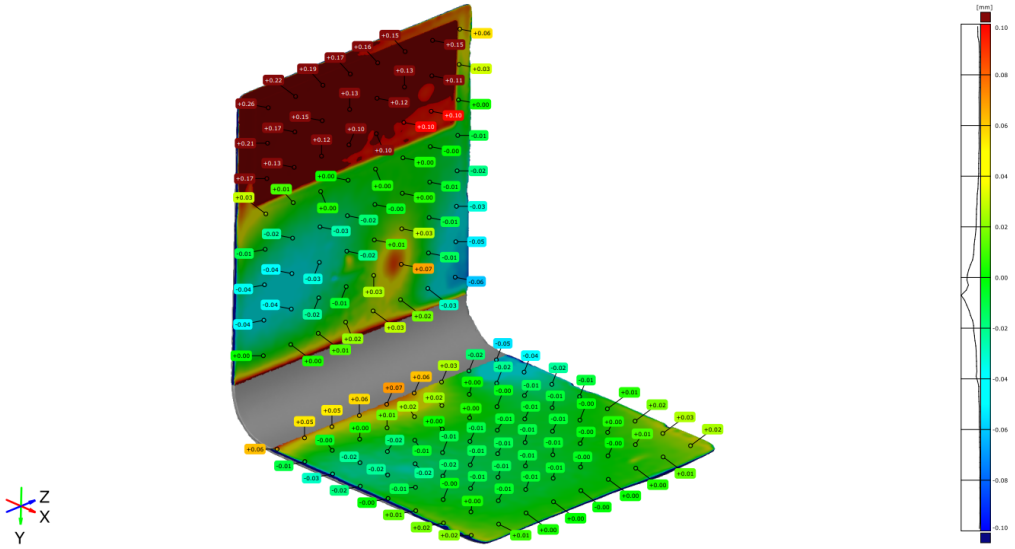

Figure B.11: Experimental measurement - Deviation to best-fit planes, $[90]_{16}$ using steel tool.

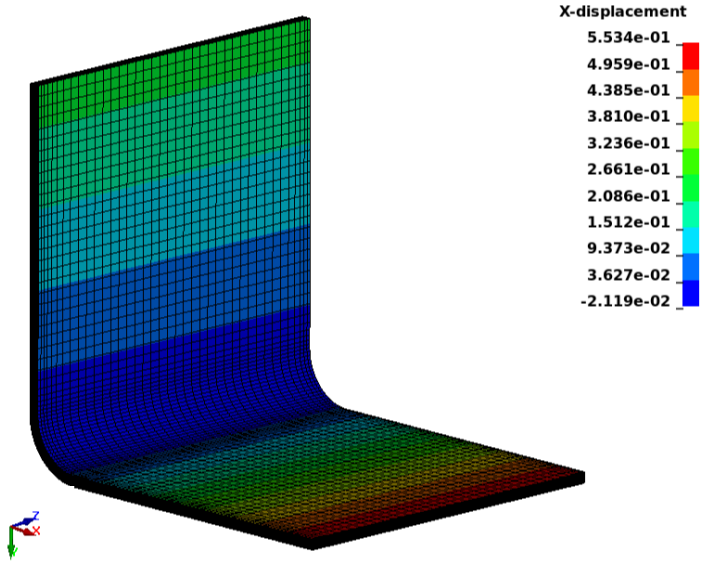

Figure B.12: Simulation result for X-displacement, $[90]_{16}$ using steel tool.

B.7 $[0/\pm 45/90/0/\pm 45/90]_S$ - Steel tool

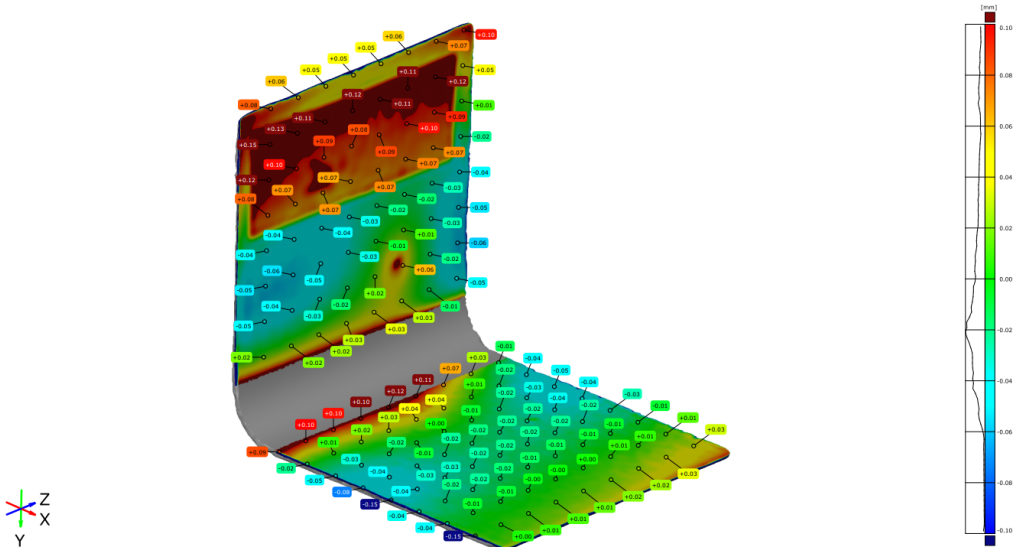

Figure B.13: Experimental measurement - Deviation to best-fit planes, $[0/\pm 45/90/0/\pm 45/90]_S$ using steel tool.

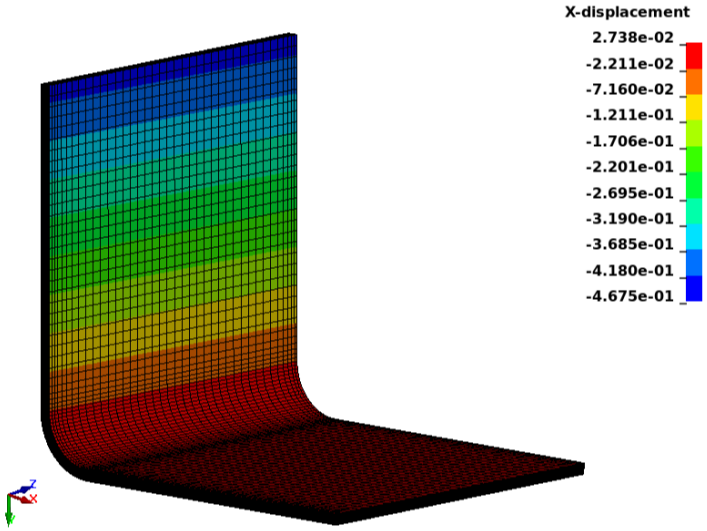

Figure B.14: Simulation result for X-displacement, $[0/\pm 45/90/0/\pm 45/90]_S$ using steel tool.

B.8 $[0/\pm 45/90/0/\mp 45/90]_2$ - Steel tool

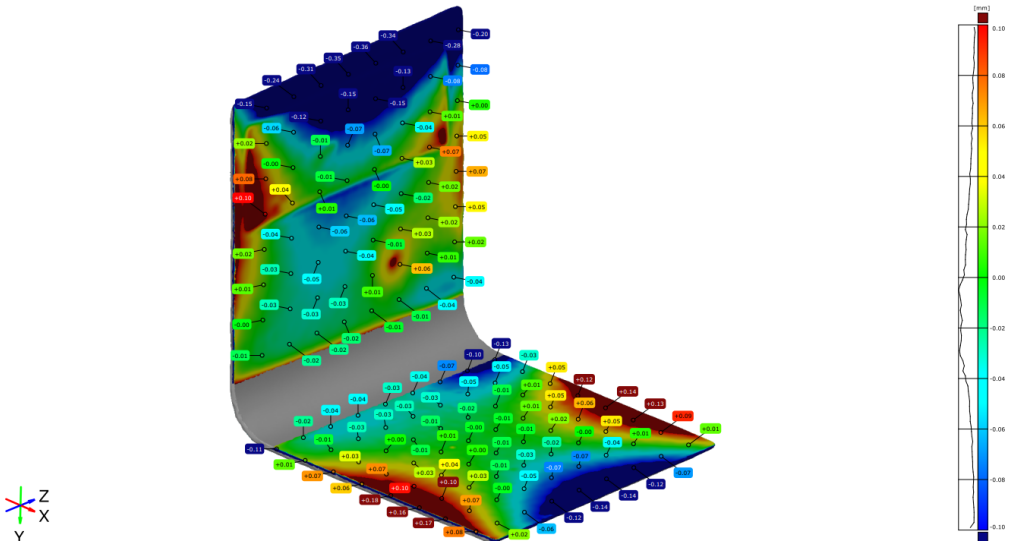

Figure B.15: Experimental measurement - Deviation to best-fit planes, $[0/\pm 45/90/0/\mp 45/90]_2$ using steel tool.

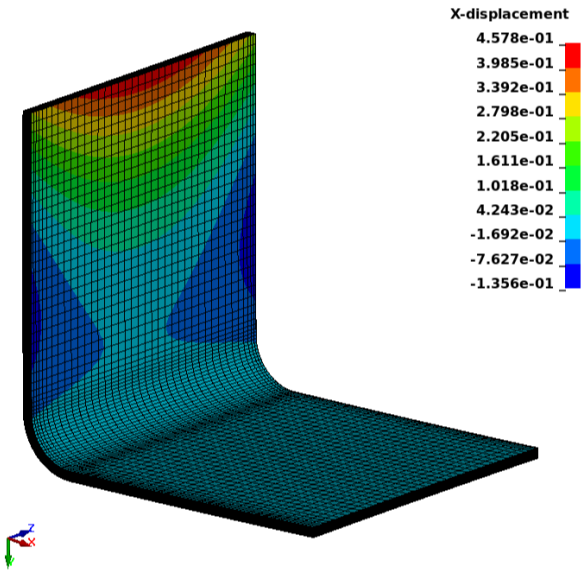

Figure B.16: Simulation result for X-displacement, $[0/\pm 45/90/0/\mp 45/90]_2$ using steel tool.

C
Appendix

Parametric Study Results

In order to determine the FE model parameters affecting the spring-in result for the fixed BC, 'tied' and sliding contact conditions, the following parametric studies were conducted. Aim of the parametric study is to achieve a 'reasonable' deviation in spring-in value among the three simulations, as it is outcome of previous studies.

The parametric studies involve:

- Variation of the element formulation (ELFORM) parameter for hexahedral elements, testing the values -2, -1, 1, and 2 following the LS-DYNA manual.
- Variation in signs of composite CTEs, tesing different combinations of signs for the three CTE parameters.
- Use of thermal contact algorithm CONTACT_AUTOMATIC_SURFACE_TO _SURFACE_THERMAL with parameters h_0, l_{min} and l_{max} set to values 0.0015, 0.1 and 0.2 respectively, as recommended by literature and LS-DYNA manual.
- Application of reasonably lower and higher cooling rate during curing.
- Variation of static and dynamic CoF (FS and FD) to realistically low values of 0.03 and 0.024, and realistically high values of 1.7 and 1.36. The empirical formula of $FD = 0.24 \cdot FS$ is still followed.
- Variation of composite CTE in three directions (CTE_a, CTE_b and CTE_c) to realistically low values of 0.1000E-6, -30.000E-6 and -30.000E-6, and realistically high values of 2.0000E-6, -40.000E-6 and -40.000E-6 in the LS-DYNA material card used.

Measuring the spring-in angle in each aforementioned simulation, the result remains the same. That indicates that probably the FE model is dependent on linear material model that is utilized, which results in no change in the spring-in.

DEPARTMENT OF INDUSTRIAL AND MATERIALS SCIENCE
CHALMERS UNIVERSITY OF TECHNOLOGY
Gothenburg, Sweden
www.chalmers.se

CHALMERS
UNIVERSITY OF TECHNOLOGY